


Doctoral Dissertation
Doctoral Program in Bioengineering and medical-surgical sciences (30th Cycle)

MECHANICAL CHARACTERIZATION OF MATERIALS AND NANO-DEVICES OF BIOMEDICAL INTEREST THROUGH NANOINDENTATION TEST

By

Gianpaolo Serino

Supervisor:
Prof. Alberto L. Audenino

Doctoral Examination Committee:
Prof. Piero Pavan, University of Padova
Prof. Gionata Fragomeni, University of Catanzaro

Politecnico di Torino

2017

Declaration

I hereby declare that, the contents and organization of this dissertation constitute my own original work and does not compromise in any way the rights of third parties, including those relating to the security of personal data.

Gianpaolo Serino

2017

* This dissertation is presented in partial fulfillment of the requirements for **Ph.D. degree** in the Graduate School of Politecnico di Torino (ScuDo).

Abstract

The nanoindentation technique, known also as instrumented indentation, has been widely accepted as a tool for the mechanical characterization of dental cement composites, and micro-devices as polymeric microspheres. The common thread through these two field is the characteristic magnitude of forces and displacements.

The only method to characterize the mechanical behavior of microspheres is the nanoindentaiton, due to their reduced size.

On the other side the cements used in dentistry are applied in thin films between a metallic support and the prosthetic crown. As well proved in literature the nanoindentation technique is the best tool to investigate the mechanical properties of thin films. Is fundamental to note that in this case the results obtained can be extended also to the bulk materials, since it be supposed that the heterogeneous composition of the cements is the same over the sample.

However, static protocols that have been developed for metals or alloys, neglecting the viscous nature of these

composites, are currently adopted in a very large body of literature.

In this study we (1) investigate how the viscous nature of dental composites could corrupt nanoindentation tests, and (2) identify an appropriate protocol that reduces the influence of the viscous, time dependent phenomenon during nanoindentation.

Here three different commercial dental cements were tested: Harvard, Telio C.S and, Temp Bond. Samples were prepared according to the procedures indicated by the manufacturers. Then, specimens were embedded in epoxy resin, cut and fine polished. Static and quasi-static tests were performed. In the static tests an input load curve was applied, that can be divided in three phases: loading, unloading and hold, where maximum load (fixed at 10 mN) was held constant. The loading and unloading rates were set as proposed elsewhere, with resulting strain rate values of 0.5, 1, 5, and 10 s^{-1}.The settings adopted for the quasi-static tests are the same as the static tests, with two substantial differences: (1) the maximum load was reached in 5 loading-unloading cycles; (2) the unloading rate was calculated based on the strain rate as measured during every hold period. The creep

data recorded during the hold phase of the static tests were fit with the Burgers model, by adding a slider.

Static tests highlighted the viscoelastoplastic nature of cement composites, indicating a strong correlation between the strain rate imposed during the loading phase and the creep rate recorded in the hold phase.

The experiments revealed that the viscous effect can be markedly minimized by applying the quasi-static approach. Moreover, the quasi-static approach allowed to obtain a reliable identification of the elastic properties of the dental composites.

By the analysis of the hold period, two creep stages can be recognized: a transient creep and a steady-state creep.

In this study we proposed a nanoindentation-based, quasi-static approach to minimize viscous effects of dental cement composites. In particular, it was demonstrated that the proposed approach is effective in minimizing the time-dependent phenomena during the unloading phase of the test. Moreover, a viscoelatoplastic model(accounting for nanoindentation test size-dependent output) wassuccessfully adopted to fit the experimental data. This model is now

suitable for computer aided simulations of the indentation process making it possible to evaluate at which level viscous phenomena could affect the estimation of the contact area.

Polymeric microspheres are largely studied for biomedical applications as, e.g., embolic agents to treat hyper-vascular tumors, or in tissue engineering. The possibility to produce an ad hoc drug delivery system is the mostly studied characteristic of these type of microspheres.

The class of polymeric microspheres used for biomedical applications are mainly composed by hydrophilic polymers, because of their biocompatibility.

Here the mechanical properties of a new design of polymeric microspheres to be used as carriers for local release of drugs and grow factors, are investigated. The rationale of the study is understand how the used polymers and the presence of the cross-linker influence the mechanical properties of the microspheres and therefore the effectiveness in properly release drugs.

The composition of the polymeric microspheres, influences their mechanical properties. Drug release experiments, performed by using methylene blue clearly

indicate that the time course of the release of the therapeutic agent strongly depends on the used polymer(s). blending natural polymers and adding genipin as natural cross-linker could lead the production of natural microspheres with adjustable mechanical properties, suitable for drug transport and delivery.

Technically, nanoindentation was applied on microspheres of size in the range 20-70 μm. The mechanical characterization highlighted a viscous-elastic behavior of microspheres, with an increasing area of the characteristics hysteresis loops when the genipin concentration increases. Moreover, on measured load-displacement data, the Hertz model was applied to estimate the Young's modulus.

A protocol for the mechanical characterization of polymeric microspheres used for drug delivery will allow: (1) to support their design phase and (2) to improve their effectiveness in targeting the release of drugs.

Acknowledgment

I would like to mention all those who helped me in writing the thesis with suggestions, criticisms and observations: to them my gratitude goes, even if I have responsibility for every error contained in this thesis.

First of all, I would like to thank professor Audenino Alberto and professor Umberto Morbiducci: without their support and their wise guidance this thesis would not exist.

I still want to thank my colleagues and friends who have encouraged me or who have spent part of their time to discuss work drafts with me.

Finally, I would like to thank the people dearest to me: my friends and my family.

alla costanza, alla pazienza

Summary

List of Figures

List of Tables

Chapter 1

Impact of Viscous Phenomena in Nanoindentation Tests of Dental Cement Composites

1.1 Introduction

Due to an increase of the demand of aesthetic and functional solutions to the pathology that bother the oral cavity, the interest on the mechanical characteristics of the materials and the methodic applied in the field of oral endodontics and oral implantology is constantly growing.

It is right and proper describe briefly the tooth anatomy, in the mouth there are four types of teeth: the incisors, the canines, the premolars and, the molars.

In Figure 1 a representation of the tooth anatomy is shown. The lower part of the tooth, the root, is placed in the bone. Between the bone and the root there is the periodontal ligament that confers a limited mobility to the tooth.

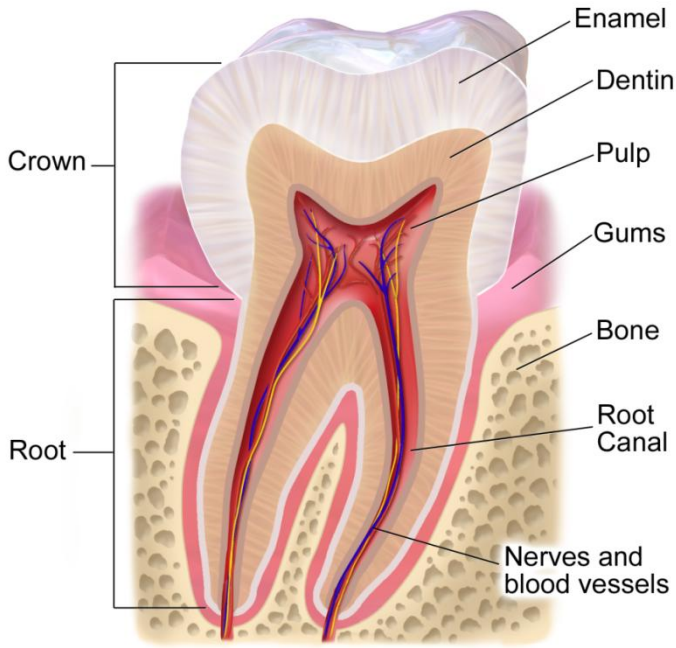

Figure 1: Anatomy of molar tooth

The exposed part is the crown that is composed by the enamel, the hardest tissue in the human body. Going inside

we find the dentin that is an hard tissue formed by tubules. The core of the tooth is the root canal were the nerves and the blood vessels are placed.

The figure below explains what is a dental implant. The implant itself is the lower part that is screwed into the bone in way to replicate the function of the root. The abutment is the connection between the implant and the dental prosthesis (or crown). Usually a film of cement is used to fix the crown to the abutment.

Figure 2: Denatal implant

The lower part that is fixed in the bone is called implant; the connection between the implant and the dental prosthesis is the abutment.

Resort to the implant occurs when there are no chances to save the entire tooth, but if the situation is not of such criticism others solutions can be contemplate, for example when only a little portion of the tooth is damaged the reconstruction is possible (veneers) or, when the machining of an important part of the natural crown is necessary, custom crowns are fixed on the natural tooth (Figure 3).

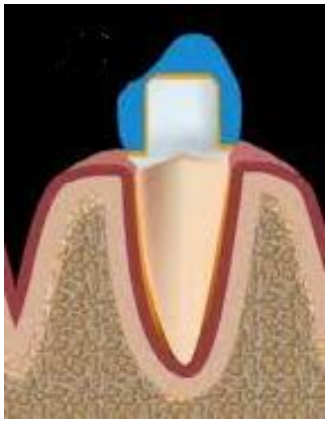

Figure 3: Prepared natural tooth for the implantation of the new crown (in blue)

Other solution more invasive than the simple restoration is the restoration through post. In this case the root channel is dug in

way to eliminate the infection and a post of appropriate materials is placed in the channel, at this point a new crown is implanted, or an ad-hoc reconstruction of the tooth is made.

All the methods briefly described above, that are only a part of the possibilities that the specialists can adopt, resorting to the use of dental cements.

In this study the indentation method will be applied to three types of cements widely used for dental restoration or in implantology. The cements are: Harvard, Telio CS Link and, Temp Bond Base. The first one is a definitive, or permanent, cement, the others two are provisional, or temporary, cements.

The provisional cements are used during the intermediate phases that follow one another; since the temporary restoration have to be removed during the treatment this kind of cements need to be characterized by a low strength. On the contrary permanent cements that need to remain in place for a long time have to be adequately strength (Ronald L. & John M., 2012).

It is clear that the mechanical properties are a crucial matter, not only for the classification of the cement itself, but also as tool for aid the design and development of the product.

1.1.1 State of art

As reported in the majority of works found in literature (Kim, Yamashita, Shotwell, Chong, & Wang, 2006) ,(Pan & Lin, 2005), (Sheets, Wilcox, & Wilwerding, 2008) (these are only few example), the characterization of the cement strength or, the evaluation of the ultimate load before the failure of the implant is done through uniaxial tests. Briefly: the restoration prosthesis are connected to the abutment (that can be the prepared tooth or the metallic part of an implant), by using a film of dental cement. Than the two components are pulled away with an international testing machine, until the separation is reached.

The flexural strength and the flexural modulus are often calculated through a three points bending tests (Braga, Cesa, & Gonzaga, 2002)(Egle Saskalauskaite, 2007). If these types of tests are performed to evaluate the elastic characteristics of the cements that could be the flexural or the Young's modulus (it depends on the type of test performed) and, the ultimate stress before the failure; the plastic characteristics of the cement are individuated through the classical tests of indentation or micro-hardness(Susannah K., Oana R., M.Hooper, & Kenneth E., 2007), (Hofmann, Papsthart, Hugo,

& Klaiber, 2001),(Yoldas & Alaçam, 2005). In this case the resistance to the penetration of the punch into the specimen is evaluated. Traditional tests of indentation are performed at the macro scale and are able to give information only about the plasticity of the material under investigation.

These types of tests are often performed to understand how a specific modification of a components of a cement or a changing of the preparation method before their application influence the mechanical characteristics of the composite. As a matter of fact, the testing phase of the cements is a fundamental step during its design and development (Ronald L. & John M., 2012). It is clear that this parameters are of crucial importance in way to enhance not only the mechanical characteristics of the cements itself but also the procedure for their application; i.e. when a particular parameter changes during the process that precedes its application the final results in terms of retention could change. As widely recognized in the literature the retention of a dental cement is strictly correlated to the mechanical properties of the cement itself: higher are the values of modulus, hardness and, ultimate strength and, better will be the retention of the cement(Cohen, Pagnillo, Newman, Musikant, & A.S., 1998).

1.1.2 Nanoindentation approach

The cement is often applied in form of a film (Ronald L. & John M., 2012) in way to join the crown to the abutment so, if the retention of the cement depends on the elastic and plastic properties, the aspect that can't be ignored is the multiphase nature of all the dental composites that strictly influence their mechanical behavior. The mechanical tests performed at the macro-scale, can't give information about the multiphase aspect of the cements, giving back results that are a summation of all the contributes of all the phases that compose the cements. The possibility to individuate the concentration of a determinate phase and how these phases contribute to the general behavior of the composite is a fundamental information for their design .

The nanoindentation technique has been widely accepted as a tool for the dental composites characterization, as proven by the multitude of works found in literature (Lixian, Longquan, L., & Danyu, 2016), (Alireza, Yasushi, Hongbing, & Junji, 2009), (Ceballos, Miguel, Victoria, & Jesus, 2007), (Toparli & N.S., 2005), (Balooch, Marshall, Marshall, S.A.S., & Balooch, 2004), (Li-Hong & Michael, 2008), (James, 2005), (Horieh, Ilnaz, Alireza, Suppason, & Junji, 2013), (Peluccio,

Bignardi, Lombardo, F.M., & Carossa, 2007). The non destructivity nature of the test, the simple process of the sample preparation, the small size required for the test, and the opportunities to evaluate the punctual mechanical characteristics are the key factor of the rapid diffusion of this method (Zhi-Quiang, Qi-Chang, Quingfeng, & Pierre, 2010). The high special resolution allow to individuate and characterize the single phases that often compose the cements (Ohyoung & Jaewoo Shim, 2001).

All the characterization technique are supported by a method (or protocol): a setting of well defined parameters that allows to perform the test in way to obtain the mechanical features of interest. Most of the works in literature characterize the composites by adopting static procedures; protocols that have been developed for metals or alloy materials that are marked by a reduced presence of viscous phenomenon. Conversely the dental composites are often affected by time dependent phenomenon (Alireza, Yasushi, Hongbing, & Junji, 2009).

The protocols are characterized by a constant loading rate value and, often the same value is used during the unloading phase; between the load and unload step there is an hold phase where the load is held constant in way to reduce the time dependent effect (Oliver & Pharr, 1992),(Hochstetter,

Jimenez, & Loubet, 1999). The only precaution is, therefore introduce an hold segment. Some time however, the introduction of this segment is not sufficient to eliminate the influence of the viscous phenomenon on the test, as observed in this study: where the creep displacement does not disappears after the hold phase, but reaches a steady state where the creep velocity become constant(Alireza, Yasushi, Hongbing, & Junji, 2009).

1.1.3 Aim of the study

As observed above all the protocols adopted for the mechanical characterization of dental cements are characterized by constant values of loading and unloading rate. Furthermore all these studies do not take into account the importance of the strain rate that, in the case of nanoindenation tests performed with tips characterized by a pyramidal like geometry, assumes a crucial role.

Previous studies on this type of cements were performed by adopting the protocols find in literature. The results, however, highlighted a dependence of the results by the loading rate

parameters and an overestimation of the mechanical properties when compared with the values found in this study.

The aim of this study, so, is to investigate how the viscosity characteristics of these composite corrupt the nanoindentation test. In particular the relation between the loading/unloading condition and the strain rate will be investigated trying to individuate an appropriate and new protocol able to reduce the affect of the time dependent phenomenon on the mechanical characterization.

The nanoindentation data will be also analyzed in way to individuate the phases that compose the cements for understand how their dispersion influences the mechanical behavior of the cements.

1.2 Materials and methods

1.2.1 Indentation theory

The application of the nanoindentaiton method for the evaluation of the mechanical properties of the elasto-plastic materials, passing for metal alloys to ceramic composite, is a well established technique; furthermore this method is largely

adopted also to characterize the behavior of viscous materials, like as polymers, resins and, tissues (from dermis to bone). The non-destructive nature of this test, the ease process of sample preparation and, its small size make this method the chosen method (Zhi-Quiang, Qi-Chang, Quingfeng, & Pierre, 2010).

Many scientists and mathematician have contributed to the develop of this technique. The first studies was conducted by Bussinesq(Boussineq, 1885) and Hertz (Hertz H. , 1882) that have studied the problem of the elastic contact. Bussineq found the relation between the stress and the displacements when a rigid axisymmetric indenter penetrates an elastic body. Hertz worked on the contact between two spherical surface with different radius. Other main contribution for the developing of the theory has been given by Sneddon (Sneddon, 1965) which was able to compute the relation between the load, displacements and contact area for different indenters which are solid of revolution and their geometry can be described by a smooth function.

Generalizing the findings of Sneddon the relation between the indentation depth and the indentation load, for punch

characterized by simple geometry, can be written as (Oliver & Pharr, 1992):

$$P = \alpha h^m$$

Where P is the indentation load, h the indentation depth and α and m are constants, that can assume different values based on the geometry of the indenter (the values are reported in the work of Oliver and Phar (Oliver & Pharr, 1992)).

It is necessary specify that was Love for the first time, to solve the problem of a "linearly elastic half-space impressed by an axisymmetric conical indenter (Zhi-Quiang, Qi-Chang, Quingfeng, & Pierre, 2010)(Love, 1939)" . Sneddon some years later gave the solution of the same problem for different axisymmetric geometries of the indenter(Sneddon, 1965).

The relation that correlates the contact pressure field along the radius of the transversal section of the conical punch found by Sneddon (Sneddon, 1965) assumes the following form:

$$p(r) = \frac{P}{\pi a^2} \cosh^{-1}\left(\frac{a}{r}\right) \tag{1.1}$$

instead the applied load vary with the indentation depth as reported in the relation (1.2)

$$P = \frac{2E^* \tan\alpha}{\pi} h^2 \tag{1.2}$$

The figure below shows how the pressure field changes along the radius of the indenter. The letter *h* indicates the indentation depth and *a* is the radius of the transverse section of the punch and α is the semi-angle of the conical tips. The area of the transversal section of the punch named "contact area" will be indicated with the letter *A*.

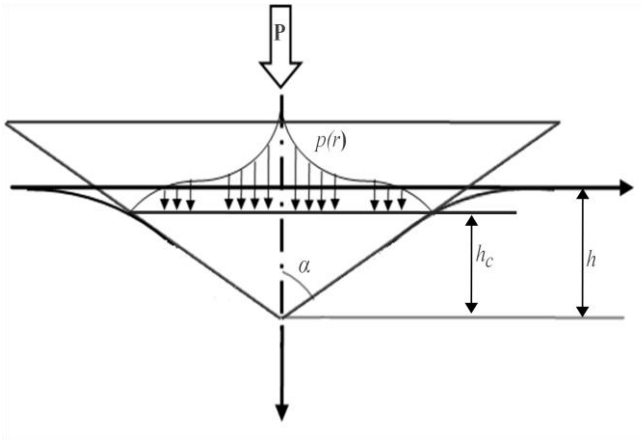

Figure 4: Contact pressure profile generated in an elastic half-space by a conical punch (view of the section parallel to the direction of loading)

The reduced (or combined) Young's modulus indicated with E^* that appear in the formula (1.2) is a combination of the Young's modulus and of the Poisson's coefficient of the material that compose the half-space. The two material parameter are combined as follow:

$$\frac{1}{E^*} = \frac{1-\nu^2}{E} \tag{1.3}$$

As reported in the work of Tabor (Tabor, 1948) when the indented material is harder enough the deformation of the indenter itself have to be taken into account and, the relation above become:

$$\frac{1}{E^*} = \frac{1-\nu^2}{E} + \frac{1-\nu_i^2}{E_i} \tag{1.4}$$

Where the parameters with the subscript *i* are referred to the material which the indenter is made. In this case the material is diamond and the parameters are the following:

$$E_i = 1141 GPa$$
$$\nu_i = 0.07$$

Differentiating the relation (1.2) with respect the indentation depth the tangent stiffness, usually called “contact stiffness”, is obtained.

$$S = \frac{dP}{dh} = \frac{4E^* Tan\alpha}{\pi} h \tag{1.5}$$

The contact stiffness (known also as unloading stiffness) is crucial for the calculation of the Young’s modulus. With simple algebraic passages the relation between the contact

area, the Young's modulus and, the unloading stiffness can be shown. The contact depth, indicated with h_c in the Figure depends by the maximum indentation depth *h* (the depth reached in correspondence of the maximum load). The relation between the two quantities is shown in the work of Sneddon[1] (Sneddon, 1965), that is:

$$h = \frac{\pi}{2} h_c \tag{1.6}$$

In correspondence of the contact depth h_c ,the contact area is defined as follow:

$$A = \pi a^2 \tag{1.7}$$

Where *a* is the radius of the transversal section of the punch in correspondence of the contact depth. Observing that the radius can be written in function of the contact depth and by adopting the relation (1.6):

$$a = h_c \tan\alpha = \frac{2}{\pi} h \tan\alpha \Rightarrow A = \frac{4}{\pi} h^2 \tan^2\alpha \tag{1.8}$$

[1] Sneddon found that the deformed profile produced by a conical indenter with a semiangle α can be expressed by the following relation: $f(x) = \varepsilon x$ where $\varepsilon = a\tan\alpha$ and $x = \pi/2$. In this case the semiangle α assume the value of $\pi/4$.

combining the equation (1.5),(1.7) and, (1.8) the unloading stiffness assume the following relation:

$$S = 2E^{*}\sqrt{\frac{A}{\pi}} \tag{1.9}$$

The unloading stiffness can be calculated experimentally, if the contact area is known, the Young's modulus can be extrapolated by the relation (1.9). The powerful feature of this findings is that, they can be applied for different geometry of the indenter (Oliver & Pharr, 2004), (Doerner & Nix, 1986). The only condition that must be respected is that the geometry of the indenter have to be a solid of revolution.

But as usual the theory that describe a phenomenon have to be adjusted to the experimental reality.

The first point that has be taken into account is the fact that the tree-sided Berkovich indenter is widely adopted for performing nanoindentation test. The mean reason, as explained in the work of Zhi-Quiang Feng et al. (Zhi-Quiang, Qi-Chang, Quingfeng, & Pierre, 2010) is due to the fabrication process. Since the material adopted is diamond, results easier grind a geometry like that shown in Figure 5 instead to create a four sided or conical indenter.

It is obvious that the Berkovich indenter does not have an axysimmetric geometry, so the relation above reported have to be adjusted. The ratio between the contact area and the contact depth has to be the same if compared with the conical indenter.

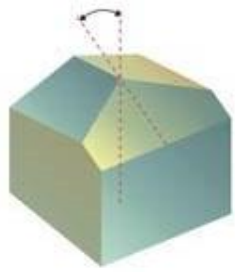

Figure 5: Tree-side Berkovich indenter

The contact area A for a tree-sided indenter can be expressed as function of the contact depth:

$$A = 3\sqrt{3}h_s^2 \tan^2\theta \qquad (1.10)$$

where θ is the face semiangle typical of a Berkovich indenter ad assumes the value of 65.27°. Comparing the contact area of the conical indenter (1.8) with the area of the tree-sided indenter (1.10) a new values of the semi-angle of the conical indenter can be found, that is 70.30°. With the new value of the angle α an equivalent area function can be obtained:

$$A = 24.5h_c^2 \qquad (1.11)$$

1.2.2 Oliver and Pharr method

The P-h curve

In Figure 6 a typical curve of an indentation test is shown.

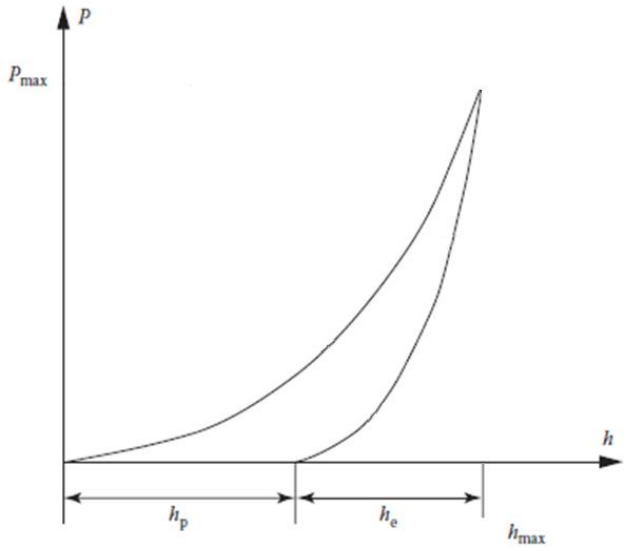

Figure 6: P-h curve obtained for an elasto-plastic material

Typically the P-h curve is characterized by two phases, a loading phase and, an unloading phase that for purely elastic material is overlapped to the curve obtained during the first phase.

It is clear that the relation between the indentation load P and the penetration depth *h* is quite different from that expected using the relation (1.2). As reported in literature during an indentation test made by a sharp indenter the plastic phenomenon develop from the early stage of the loading phase simultaneously to the elastic deformation, on the contrary the unloading phase is characterized only by the elastic recovery (Oliver & Pharr, 1992).

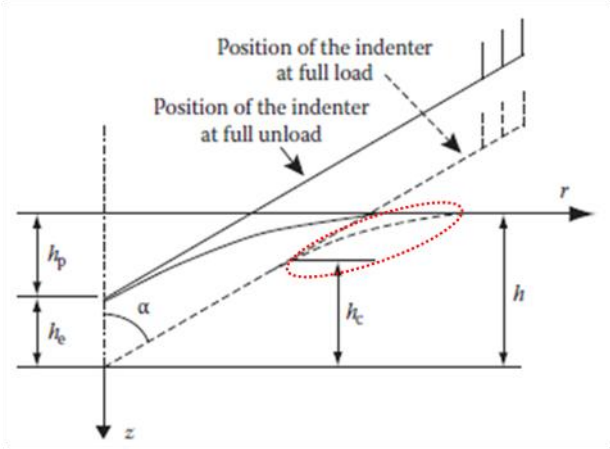

Figure 7: Nanoindentaiton process at a maximum load (dotted line) and at the end of the unloading phase (solid line)

Figure 7 (Zhi-Quiang, Qi-Chang, Quingfeng, & Pierre, 2010) clarifies the meanings of the quantities h_p, h_e and, h_c. The value of h_c indicates the contact depth; in detail is the portion of the tip that is in contact with the sample. The quantity h_e

indicates the recovery of deformation and is obtained by subtracting from the maximum value of the indentation depth the plastic portion of the deformation (h_p). In the light of the fact that the plastic phenomenon can be neglected during the unloading phase(Sneddon, 1965), the relation above introduced can be applied only during the unloading phase.

Another fundamental aspect is the bending of the surface (highlighted by the dotted circle in Figure 7). The portion of the tip in contact with the sample does not correspond with the indentation depth registered during the test. The displacement generated by the bending of the surface (denoted with h_s) have to be subtracted by the total displacement. Now arise the problem of define this quantity that, how reported by Oliver and Pharr in one of their first and more relevant work (Oliver & Pharr, 1992), changes with the indenter geometry. The relation found by Sneddon (Sneddon, 1965) for a conical indenter can be used for calculate the displacement along the z-axis that corresponds to the bending of the surface:

$$h_s = \frac{(\pi - 2)}{\pi}\left(h - h_f\right) \tag{1.12}$$

where h_f correspond to h_p. The quantities (h - h_p) for the sake of the exposition the quantities h_f is substituted with h_p -, has been calculated by Sneddon through the following expression:

$$\left(h - h_p\right) = 2\frac{P}{S} \tag{1.13}$$

where S is the unloading stiffness and P is the indentation load registered in correspondence of the maximum indentation depth. The relation becomes:

$$h_s = \varepsilon \frac{P_{\max}}{S} \quad \left(\varepsilon = \frac{2}{\pi}\left(\pi - 2\right)\right) \tag{1.14}$$

Using the same approach similar relation can be obtained for others axisymmetric geometries i.e., the values of the geometric constant ε become 1 for a flat punch and 0.75 for a paraboloid of revolution (Oliver & Pharr, 1992),(Oliver & Pharr, 2004).

Mechanical parameters estimation

At this point the true powerful of the method proposed by Oliver and Pharr for the analysis of the data obtained through instrumented nanoindentantion can be understood. If a fine

calibration of the indenter transversal area is made (the question will be treated further in this discussion), and the values of indentation contact depth h_c is correctly estimated, a fine tool for a very rapid calculation of the hardness and Young's modulus is obtained. When these information are available there is no need to capture the image of the residual impression left by the indentation, for the calculation of the contact area.

The relation that defines the nanoindentation hardness is the same used in the case of macroscopic indentation:

$$H = \frac{P_{\max}}{A(h_c)} \tag{1.15}$$

but, as can be noticed the transversal area is now function of the indentation depth.

As regard the elastic properties, recalling the relation (1.9), it is clear that the Young's modulus can be calculated when the value of the unloading stiffness is known.

It is right and proper, clarify that Sneddon's results reported above hold only for the elastic portion of the contact, so the unloading stiffness have to be calculated, only on the last stage of the indentation test where the elastic part of the deformation is recovered. The matter of the problem, now, is

how to properly choose the way to calculate the unloading stiffness. Roughly speaking the unloading stiffness calculation could be extrapolated through a straight line that fit the upper portion of the unloading curve and, calculating the slope of the fitted line. For non linear unloading curves rise the questions on how many of the unloading curve and where have to be taken the data for the calculation of the slope. The experimental reality revealed that this kind of approach does not give consistent results when the data used for the linear fitting changes (Oliver & Pharr, 1992).

As explained by Oliver and Pharr the incoherence of the unloading stiffness values is due to the creep that characterize the first part of the unloading curve; this is the reason for what all the indentation protocols are provided of an hold period prior the onset of the unloading phase. In this way the time dependent phenomenon should reduce in way to not affect dramatically the calculation of the unloading stiffness. At the same time the two scientists have shown that the unloading curves obtained for different materials is well approximated by a power law relation of this kind:

$$P = \alpha \left(h - h_p \right)^m \tag{1.16}$$

where α, m and, h_p are constants of the power law fitting model. In this way the unloading stiffness can be calculated analytically. The derivative evaluated by differentiating the relation (1.16), explain the two scientists, seems not be corrupted by the time dependent phenomenon; i.e. the derivative calculated at the peak load ,using the upper portion of unloading data for the power law fitting, varies of a small amount when compared with the derivative calculated by taking into account the last portion of unloading data (Oliver & Pharr, 1992).

Last consideration worthy of note is the introduction of the β factor. This factor takes into account all the experimental reality that the model does not consider. If the bending of the surface is considered by introducing the factor ε, the end rounding of the Berkovich indenter tip, as well as the non axisymmetric geometry are taken into account by the parameter β. The assumptions made on the indenter geometry on which the model has been developed is in contrast with the experimental realty. Different works have been done to correct the model but the results are very different (Oliver & Pharr, 2004),(King, 1987), (Bolshakov & Pharr, 1998)(Hay, Bolshakov, & Pharr, 1999)(Cheng & Cheng, 1998)(Cheng & Cheng, 1999)(Larsson, Giannakopoulos, Soderlund,

Rowcliffe, & Vestergaard, 1996).Values of β often used are 1.034 or1.05. The relation adopted for the calculation of the unloading stiffness becomes:

$$S = 2\beta E^* \sqrt{\frac{A}{\pi}} \qquad (1.17)$$

1.2.3 Nanoindentation system

All tests were performed with a Nanoindenter XP (MTS/Agilent, USA), equipped with a diamond Berkovich indenter.

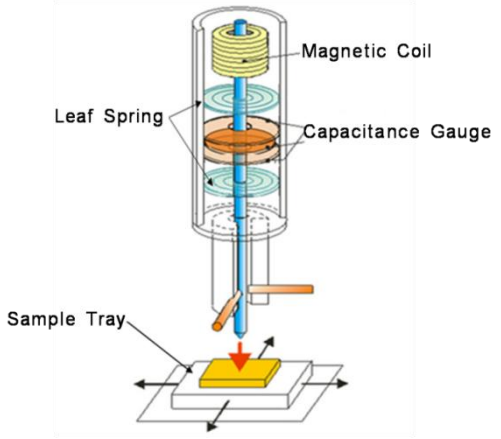

Figure 8 Schematization of the Nanoindenter. The magnetic coil moves the tip, the displacement capacitance sensor allow the

fine detection of the tip displacements, the sample tray moves the sample on the plane and leaf springs avoid the lateral movements

The Figure 8 represents a schematization of the working principle of the instrument. The load is imposed through a magnetic coil (the working principle is based on the Lorentz force) and the displacement of the tip is registered by using the capacitance gauge. The leaf spring is characterized by a very low stiffness in the direction of force application and a very high stiffness in the direction perpendicular to the indenter shaft in way to reduce the lateral movement. The sample is moved through a screw-driven system.

The systems adopted to apply the force, to sense the displacement and to move the sample allow to obtain the following resolution values: the smallest value of force that can be applied is of 50 nN; the minimum value of displacement that can be detected is less than 0.01 nm; and the position of the indentation site can be chosen with a resolution of 45 nm and an accuracy of 1.5 μm.

The indentation sites can be chosen by using the optical microscope embedded in the nanoindenter.

Before every test the offset between the indenter tip and the microscope has been finely calibrated. The calibration procedure is performed on an aluminum disk. The high

plasticity of this material makes the identification of the imprint unequivocal.

1.2.4 Tip calibration

The tip calibration is a crucial procedure that have to be executed before performing indentation test, the accuracy of the results will be strictly correlated to the calibration procedure (Oliver & Pharr, 1992),(Oliver & Pharr, 2004). As reported in the section -Indentation Theory- one of the advantages of the method proposed by Oliver and Pharr resides in the fact that the transversal area can be calculated as function of the indentation depth. Differently from the traditional indentation test, where the imprint leaves by the punch have to be measured through optical technique, in this case the contact area can be expressed as function of the indentation contact depth as follows:

$$A(h_c) = 24,5h_c^2 + C_1h_c^1 + C_2h_c^{1/2} + C_3h_c^{1/4} + ... + C_8h_c^{1/128} \quad (1.18)$$

The polynomial coefficients do not have a physical meaning. The coefficients of higher order are used for fit the non ideal tip shape of the indenter punch. The first coefficient is

constant and is predominant when the indentation is performed in deep. Usually only the first five coefficients are taken into account during the calibration procedure.

The calibration procedure is made on a sample of standard materials, that is fused silica. This material is chosen for its isotropic characteristics and a well defined values of Young's modulus and hardness. The calibration procedure (the determination of the coefficient values) is based on an iterative procedure, based on two key information: the value of the Young's modulus, and the value of the frame stiffness. The iterative procedure is extensively explained in the work of Oliver and Pharr (Oliver & Pharr, 1992).

1.2.5 Materials

Here three different commercial dental cements were tested, in particular two types of cements used in different stage of the dental restoring. The permanent cement Harvard® (Harvard Dental International GmbH, Germany) [2] and, the temporary cements: Telio C.S® (Ivoclar Vivadent,

[2] All the information are obtained by the datasheet products

Liechtenstein)[2] and, Temp Bond® (Keer Italia s.r.l., Salerno, Italy)[2].

In detail the Harvard cement is initially separated in solid and liquid phase. The solid phase is a powder; 1 gr of the powder is for the 86% zinc oxide and, for the 8.6% magnesium oxide. 1 gr of the liquid phase contains for the 56% o-phosphoric acid. The cement can be used for fixing the crowns and multiple bridges on implants or on the natural teeth. Other applications are luting of inlays, cavity linings, temporary fillings in posterior teeth, reconstruction of the core and, orthodontic works.

Telio CS Link cement is a dual curing (light and self-curing) temporary composite, it is used for temporary cementation of provisional crowns, bridges, inlays, onlays and veneers. This cement can be adopted also in combination with resin-based crown. The composition of the cement is for the 56 wt. % bismethacrylates and fillers for 43 wt. %: additional elements are initiators, stabilizers and pigments.

The Temp Bond Base cement is composed for the 85-90% Zinc Oxide and is applied for temporary solution.

1.2.6 Samples preparation

The cement samples were prepared following the procedure indicated by the manufacturer, in way to obtain little column of composite (0.5 cm the radius of the circular section, and 2 cm in length). The specimens have been embedded in epoxy resin and cut.

The surface roughness (Ra) of the samples has been evaluated through a profilometer. The first measures have shown that the Ra values calculated are not compatible with the standard ISO 14577, or with indentation depth reference value of 20 R_a (Mahalia, Christopher, Matthieu, & Franz-Josef, 2008). Values of R_a less than 0,2 µm have been obtained by polishing the sample using sand paper disks of decreasing grit size and using a polishing diamond paste. The debris have been removed trough pressurized air.

1.2.7 Static tests

A typical indentation test is characterized by an input curve composed by tree steps:

Loading step: the tip moves downward until the contact is detected (the nanoindenter discriminate the contact when the derivative of the load with respect the displacement exceed a threshold value). At this point the test begin and the force is incremented at the prescribed value of loading rate.

When the defined maximum value of load has been reached an holding phase is performed, the load is held constant for a fixed time interval. The hold period is of crucial importance for the reduction of the time dependent phenomenon (Hochstetter, Jimenez, & Loubet, 1999)

After the holding phase the tip is usually retracted, at the same rate imposed during the loading phase.

The parameters that have to be set in this case are the maximum indentation load and the loading/unloading rate.

Tests have been performed controlling the load indeed, a maximum value of 10 mN has been chosen for all the tests. Such value of load is prescribed by the Ra measured value: 10 mN is the limit value of indentation load that allow to obtain a value of indentation depth compatibles with the Ra value. Preliminary nanoindentation tests were performed on all cements for individuate the best value of maximum indentation load.

Supposing that the material characteristics do not vary during the testing period, in particular the hardness, is the only hypothesis made for defining the loading\unloading rate values. As shown by the works of G. Hochstetter et al. (Hochstetter, Jimenez, & Loubet, 1999) and B. N. Lucas et al. (Lucas, Oliver, Pharr, & Louber, 1997) to held a constant values of the hardness when the indentation depth changes it is essential set a constant strain rate, the punch have to be pressed in the surface specimen in such a way to obtain a constant strain rate. Starting by the formula for the calculus of the hardness the value of loading rate that allows to held the strain rate constant can be calculated (Lucas, Oliver, Pharr, & Louber, 1997).

$$H = \frac{P}{A} = \frac{P}{ch^2} \tag{1.19}$$

The transversal area of the tip, can be expressed in function of the indentation depth *h*, so the load assumes the following relation:

$$P = ch^2 H \tag{1.20}$$

differentiating the load respect the time, the relation (1.21) is obtained.

$$\dot{P} = ch^2 \dot{H} + 2ch\dot{h}H \tag{1.21}$$

The expression of the variation of the displacement with the time can be written:

$$\dot{h} = \frac{\dot{P}}{2chH} - \frac{ch^2 \dot{H}}{2chH} \tag{1.22}$$

Dividing the (1.22) for the displacement *h* the expression of the strain rate is obtained:

$$\frac{\dot{h}}{h} = \frac{\dot{P}}{2ch^2 H} - \frac{\dot{H}}{2H} \tag{1.23}$$

For the (1.20), the expression of the strain rate become:

$$\frac{\dot{h}}{h} = \frac{1}{2}\left(\frac{\dot{P}}{P} - \frac{\dot{H}}{H}\right) \tag{1.24}$$

Since the hardness does not vary with the time the loading\unloading can be defined as follows:

$$\dot{P} = 2\frac{\dot{h}}{h}P \tag{1.25}$$

Different values of loading\unloading rate have been obtained imposing different values of strain rate. Four are the values of strain rate imposed: 0.5, 1, 5 and, 10 s^{-1}. The higher values of strain rate are imposed in way to identify the viscous behaviour of the composites during the holding phase

(Marezan, Beyaoui, Bigerelle, & Guigon, 2012), it is well known that for reduce the effect of time dependent phenomenon during an indentation test the strain rate have to be low (Tang & Ngan, 2003), (Cheng, Cheng, & Ni, 2005).

Defining the loading rate as in the (1.25) a constant value of the hardness is obtained even if the indentation depth used for the transversal area calculation is different (Lucas, Oliver, Pharr, & Louber, 1997).

It is essential to note that differently by the method applied in literature, is the strain rate constant and not the loading\unloading rate. As argued above a constant value of strain rate permits to keep the hardness value independent by the indentation depth, ensuring that the rate of tip penetration remains constant. Adopt a constant loading\unloading rate could be correct when the transversal area of tip is constant, if the hardening of the material under the tip is ignored.

1.2.8 Viscoelastoplastic (VEP) model

The displacement registered during the hold phase of the static test, that is the creep of the composite, has been

analyzed trough the Burgers model (Chien-Chao, Mao-Kuo, & Sanboh, 2011), (Chien-Kuo, Sanboh, Li-Piin, & N, 2006). The Burgers model is a combination of the two well known model, the Kelvin-Voigt model and the Maxwell model. These two models are a combination of elementary systems which identify the mechanical properties of materials. For the analysis of the data obtained by a nanoindentation experiments the linear elements (spring, dashpot and slider) have to be adjusted to the quadratic relation that exists between the load and the displacement typical of a nanoindentation experiment (Marezan, Beyaoui, Bigerelle, & Guigon, 2012), (Oyen & Cook, 2003)(Oyen-Tiesma, Tivola, & Cook, 2001), (Olesiak & Oyen, 2010). The linear elements can be used only for flat punch, since the relation between the indentation load and the indentation depth is linear, as shown by (Doerner & Nix, 1986).

Recurring to the results of Sneddon (Sneddon, 1965) the relation between the indentation load and the indentation depth for a perfect conical indenter can be considered quadratic (Oliver & Pharr, 2004).

$$P(h) = \alpha h^2 \tag{1.26}$$

For the (1.26), the relation for the spring, dashpot and slider become respectively (Olesiak & Oyen, 2010), (Chien-Kuo, Sanboh, Li-Piin, & N, 2006), (Marezan, Beyaoui, Bigerelle, & Guigon, 2012).

$$\begin{aligned} P_p(h) &= \alpha_1 H h_p^2 \\ P_e(h) &= \alpha_2 E^* h_e^2 \\ P_v(h) &= \alpha_3 \eta_Q \left(\frac{dh}{dt}\right)^2 \end{aligned} \tag{1.27}$$

Where the α_i coefficient are geometrical constant defined by Oyen and Cook (Olesiak & Oyen, 2010) and the numerical values assigned are 24.5 and 4.4 respectively for α_2 and for $\alpha_1 (= \alpha_3)$.

The Figure 9 shows the model.

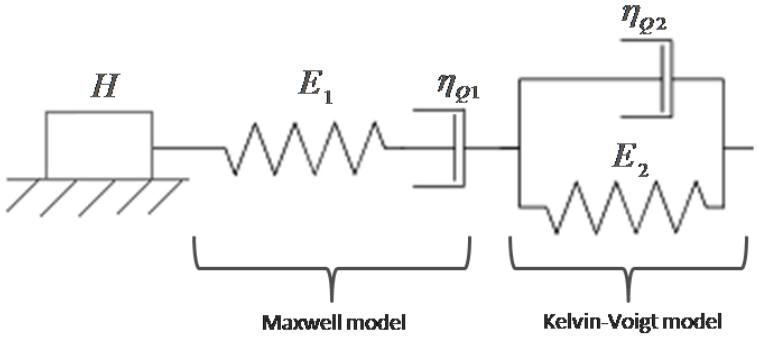

Figure 9: Viscoelastoplastic (VEP) model

The Burgers model has been modified considering also the energy dissipation due to the plastic deformation so, a slider has been added to the model has done in the other works(Marezan, Beyaoui, Bigerelle, & Guigon, 2012), (Oyen-Tiesma, Tivola, & Cook, 2001),(Olesiak & Oyen, 2010).

The total displacement of the model can be defined as:

$$h_{tot} = h_e + h_v + h_p + h_{ve} = h_{vp} + h_{ve} \tag{1.28}$$

Where for simplicity the displacement indicated with h_{ve} is the viscoelastic displacement of the Kelvin-Voigt model, and the displacement h_{vp} is the sum of the displacement of the Maxwell model and of the slider. The superimposition of the displacement described by the combination of the system in Figure 9 is valid for the assumption that the materials are characterized by a linear viscoelasticity(Alireza, Yasushi, Hongbing, & Junji, 2009).

Applying the model for analyze the indentation displacement during the hold phase the application of the load has been considered instantaneous, so the elements of the Kelvin-Voigt model can't respond immediately to the stress for the presence of the dashpot; in other words:

$$h_{ve}\big|_{t=0} = 0 \tag{1.29}$$

The instantaneous response is held by the elastic element of the Maxwell element. The displacement at the time t = 0 can be written as follow:

$$h_{vp}\Big|_{t=0} = \sqrt{\frac{P_{\max}}{\alpha_2 E_1^*}} \tag{1.30}$$

The displacement h_{ve} can be calculated from the following equation:

$$\sqrt{P} = \sqrt{\alpha_2 E_2^*}\, h_{ve} + \sqrt{\alpha_3 \eta_{Q2}}\, \frac{dh_{ve}}{dt} \tag{1.31}$$

The solution of the differential equation of the first order combined with the (1.29) gives the following expression of the h_{ve} displacement during the hold segment:

$$h_{ve}^{creep}(t) = \sqrt{\frac{P_{\max}}{\alpha_2 E_2^*}} \left(1 - e^{-\frac{t}{\tau}}\right) \tag{1.32}$$

where the time constant τ is the ratio:

$$\tau = \sqrt{\frac{\alpha_3 \eta_{Q2}}{\alpha_2 E_2^*}} \tag{1.33}$$

The displacement h_{vp} can be derived with respect the time:

$$\frac{dh_{vp}}{dt} = \frac{dh_e}{dt} + \frac{dh_v}{dt} + \frac{dh_p}{dt} \tag{1.34}$$

For the (1.27), the expression (1.34) can be rewritten as:

$$\frac{dh_{vp}}{dt} = \sqrt{\frac{P_{\max}}{\alpha_3 \eta_{Q1}}} \tag{1.35}$$

The integration of the (1.35) and the (1.30) gives the following expression of the displacement h_{vp}:

$$h_{vp}^{creep} = \sqrt{\frac{P_{\max}}{\alpha_3 \eta_{Q1}}} t + \sqrt{\frac{P_{\max}}{\alpha_2 E_1^*}} \tag{1.36}$$

Superimposing the displacement (1.32) and (1.36), the complete expression of the creep displacement predicted by the model is obtained:

$$h^{creep} = \sqrt{\frac{P_{\max}}{\alpha_3 \eta_{Q1}}} t + \sqrt{\frac{P_{\max}}{\alpha_2 E_1^*}} + \sqrt{\frac{P_{\max}}{\alpha_2 E_2^*}} \left(1 - e^{-t/\tau}\right)$$

$$h^{creep} = \sqrt{P_{\max}} \left[\sqrt{\frac{1}{\alpha_3 \eta_{Q1}}} t + \sqrt{\frac{1}{\alpha_2 E_1^*}} + \sqrt{\frac{1}{\alpha_2 E_2^*}} \left(1 - e^{-t/\tau}\right) \right] \tag{1.37}$$

1.2.9 Quasi-static tests

Quasi-static tests are cyclic tests where the maximum loading value is reached in different steps. In this case the test is characterized by 5 cycles and for every cycles an increment of

2 mN in the load is set, in way to reach a maximum load value of 10 mN.

As notice during the static tests, the displacement registered during the hold period changes with the different values of strain rate imposed, i.e. the length of the hold period depends on the value of strain rate imposed. In the light of that, the idea is to evaluate the strain rate during the hold period and, define the unloading rate by using the estimated strain rate value.

A customized function has been built for the calculation of the strain rate. The discrete derivative of the displacement channel (the displacement channel measures the penetration of the punch in the cement) with respect the time was implemented, and normalized respect the displacement itself.

During the test five cycles have been performed, this means that for one test of this kind five unloading phases can be recognized and so 5 values of Young's modulus can be calculated, property that is strictly influenced by the time dependent phenomenon; as shown by the analysis of the static tests. The cyclic test allows, indeed, to monitor how the elastic properties vary with time and with the strain rate evaluated during the hold period.

As regard the loading rate, it was defined in the same way of the static tests; strain rate values chosen for set this parameter are the same of the static tests, namely: 0.5, 1, 5 and, 10 s^{-1}.

1.2.10 Statistical analysis

Batch constituted by a matrix of 40 indentations, equally distant of 50 μm, have been preliminary analyzed with the modified Thomposon tau test in way to identify the outliers.

The analysis of variance (ANOVA) at one way was performed to analyze the influence of the experimental setting on cements' mechanical properties. The Young's modulus and the hardness (the parameters) have been analyzed separately. The strain rate imposed was considered as the factor.

1.3 Results and discussions

The static tests highlight the viscous nature of these composite, and highlight the critical issues related to the application of such type of method. Moreover a raw analysis of the time dependent phenomenon is made observing the evolution of the displacement registered during the holding stage imposed after the loading phase.

The application of the VEP model to the displacement registered during the first holding phase of the static test, could clarify the role of time dependent phenomenon during the holding and the following unloading phase.

Finally the results obtained by the application of the new method here proposed will be shown.

1.3.1 Static tests

Harvard

Representative curves of static tests performed on the Harvard composite are shown in Figure 10. The curves highlight the plastic and viscoelastic behavior of the cement since only a portion of deformation is recovered, instead during the two hold phases is possible observe the viscous characteristic. So the composite when stressed respond with three different mechanism.

The curves here reported clearly show the influence of the loading rate during the experiments. Observing the loading phase, can be recognized a stiffening of the cement: higher is the loading rate and less results the maximum value of the indentation depth reached before the hold phase.

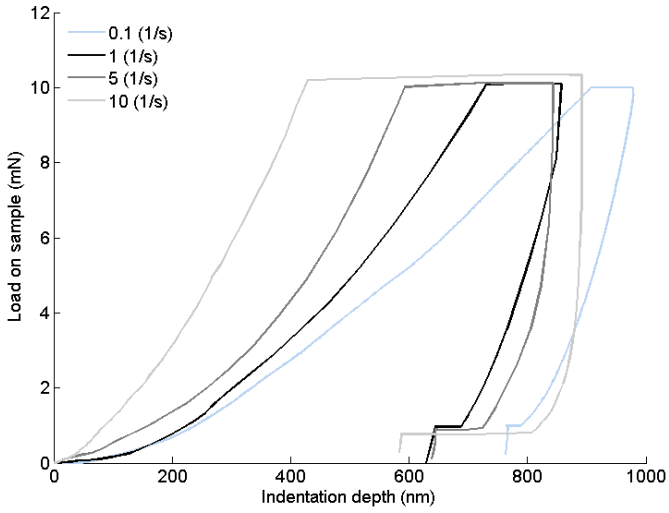

Figure 10: Representative curves of static test performed on Harvard cement, selecting 4 different value of loading/unloading rate

The response of the composite during the first hold period is opposite to that expected observing the behavior of the cement during the loading phase: the displacement registered during the hold step increase with the loading rate.

The penetration of the tip during the hold phase, measured by the length of the hold period, is strictly correlated to the creep rate, that increases when the loading/unloading rate rises(Zhang, Shao, Li, & Jiang, 2016).

The hold period, as reported in other work,(Zhang, Shao, Li, & Jiang, 2016), (Briscoe, Fiori, & Pelillo, 1998) is a stabilization period essential for the complete development of the time dependent phenomenon and for a correct evaluation of the mechanical properties. As a matter of fact, during the unloading phase the curves do not show the typical nose that appears when viscous phenomena are evolving at the beginning of the unload phase (Briscoe, Fiori, & Pelillo, 1998), (Chien-Kuo, Sanboh, Li-Piin, & N, 2006).

The second holding phase does not influence the calculation of the elastic and plastic properties, and is a build up feature of the program for the definition of the thermal drift. The thermal drift in this case has not been processed, since for viscous materials the creep registered during the holding phase for the thermal drift calculation could not be due to the temperature variation. It can be noticed as well, from Figure 10 that the recovery of the deformation is more pronounced when the unloading rate increases, indicating that the viscous phenomenon still influence the unloading phase, nevertheless the presence of an hold period just prior of the unloading step.

A quantitative evaluation of the elastic (Young's modulus) and plastic (hardness) properties of the material are reported in Figure 11.

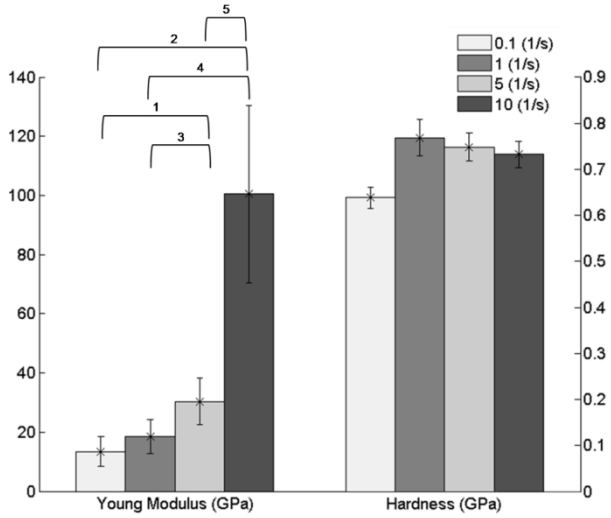

Figure 11: Left side: Average values of Young's modulus calculated for four different values of unloading rate. Right side: Average values of hardness calculated for four different values of loading rate. Statistical significant differences between mechanical characteristics and strain rate are reported. The bars indicate the statistical influence of the loading/unloading rate and the p-values calculated ($1\text{-}1.37265\cdot10^{-11}$; $2\text{-}2.968041\cdot10^{-21}$; $3\text{ - }4.25618\cdot10^{-9}$; $4 - 1.03664\cdot10^{-20}$; $5 - 1.00887\cdot10^{-18}$) by using the ANOVA analysis with a confidence interval of the 95%

The Young's modulus increases when the loading rate rise. Significant differences are highlighted by the ANOVA analysis for values of Young's modulus obtained for strain

rate values higher than 0.1 s^{-1}. The hardness, instead, is not influenced by the changing of the loading rate. Only a small increases is registered for values of strain rate higher than the lowest one, as a matter of fact the statistical analysis does not show significant differences of the obtained hardness values for increasing values of the strain rate (p-value 0.3781). Observing the load-displacement curves in Figure 10 the statistical independence of the hardness parameter from the strain rate values imposed is explained by the fact that the indentation depth reached after the holding phase (max indentation depth) is stable (except for a little variation registered for the value of strain rate equal to 0.1 s^{-1}).

For increasing values of strain rate the penetration (primary creep rate) of the indenter at the beginning of the hold phase becomes even more fast, in particular an increasing of the rate calculated during the primary creep is registered for increasing values of the strain rate. Observing that the stress filed underneath the tip follows the same trend of the primary creep rate (the registered deformation, and so the cross section of the tip, in correspondence of the maximum load decrease when the loading rate increase), it can be stated that the increase of the penetration rate registered during the early stage of the first hold phase is strictly connected to the stress

field, as found, also, in literature (Whittaker, Harrison, Deen, Rae, & Williams, 2017).

Stable values of the max indentation depth therefore are due to increasing values of the stress field underneath the tip, obtained for increasing values of strain rate. As argued by Oliver and Pharr (Oliver & Pharr, 1992) the hold period permit the development of the plastic time dependent phenomenon in way to obtain a right and proper value of hardness.

How the elastic property and the unloading rate are linked can be explained by plotting the obtained values of Young's modulus and the selected values of strain rate, as reported in Figure 12. Interpolating the data with an exponential model a good agreement is found $\left(R^2 = 0.9933\right)$. The composite become even more stiffer when the unloading rate increases following an exponential trend.

Elastic properties are dramatically influenced by the variation of the strain rate imposed for the calculation of the values of loading and unloading rate. The unloading stiffness calculated during the unloading phase is strictly correlated to the creep of the material(Oliver & Pharr, 1992), in other wards the time

dependent phenomenon play a crucial role during the first stage of the unloading phase. The data shown in the histogram indicate that higher is the creep and higher will be the unloading stiffness.

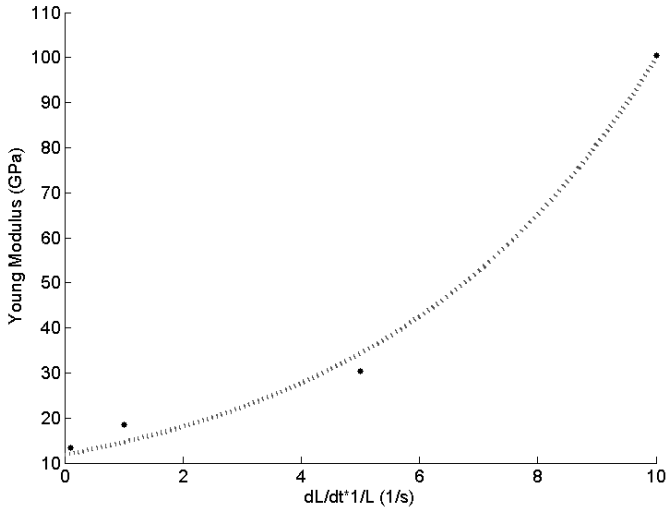

Figure 12*:* Black dots represent the mean value of the Young's modulus; dotted line represents the fitting exponential model

Further analysis later presented will clarify the role of the creep during the unloading on the evaluation of the Young's modulus.

Furthermore it is possible correlate the dependence of the elastic behavior to the strain rate, observing that the tensional state generated underneath the tip during the loading phase of

the nanoindentation test, as reported in literature (Chang & Zhang, 2009), (Vladislav, Gogotsi, & Dub, 2000), (Schuh, 2006), generates a phase transformation of the elements that constitute the cement modifying as a consequence the shape of the loading/unloading naonidentaton curves, from which the Young's modulus is obtained. In the light of that is possible correlate the dependence of the values of Young's modulus to the strain rate that influence the stress field underneath the tip.

Other fundamental aspects is the composition of these types of samples. The cements under investigation are produced by mixing different materials with different mechanical characteristics.

For composite materials the indentation technique is very powerful, the reduced size of the diamond tip permit to individuate the distribution of the mechanical properties in a predefined area. In Figure 13 the histogram and the distribution probability function (PDF) of the hardness is shown.

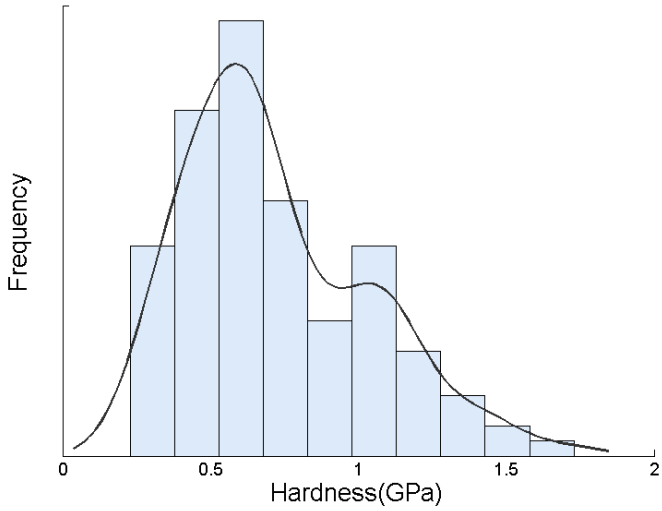

Figure 13: Histograms and probably density function (solid line) of hardness obtained for four values of stain rate. A- $0.1\left(1/s\right)$;B- $1\left(1/s\right)$; C- $5\left(1/s\right)$; D- $10\left(1/s\right)$

The histogram includes the distribution of the mechanical properties in four different areas of the sample, calculated for four different values of strain rate, the combination of the values of all tests has been possible for the independence of the hardness by the strain rate. The bimodal distribution of the hardness explains the dispersion of the two main components of the cement. The higher number of observations is obtained for the lowest value of the hardness indeed, the mean value of hardness with higher observation is related to the zinc oxide, the lowest peak is related to the magnesium oxide, namely the

distribution of the hardness values reflects the composition of the powder used for the preparation of the composite.

Telio CS Link

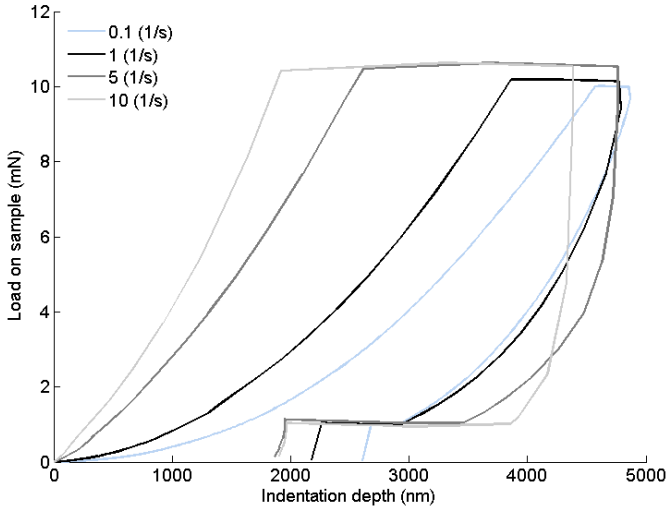

Figure 14: Representative curves of static test performed on Telio CS cement, selecting 4 different value of loading/unloading rate

Analogous experiments were performed on the Telio CS cement. Static curves representative of all tests are showed in Figure 14.

Differently to the results reported for the Harvard cement, in this case the indentation depth increases considerably even if

the parameters of the method are the same. The cement is characterized by a reduced resistance to the penetration of the indenter, when compared with the Harvard cement. The composite, as well as the Harvard cement, is characterized by a plastic and viscoelastic behavior. The stiffening of the cement during the loading phase for increasing values of the loading rate is clear. As observed for the previous analyzed composite, a counterintuitive evolution of the hold phase is registered. the penetration of the tip during the hold phase is strongly correlated to the primary creep rate (Zhang, Shao, Li, & Jiang, 2016): higher is the strain rate and higher will be the primary creep rate, for this reason the hold segment become even more pronounced when the strain rate increases. For materials that exhibit viscous characteristics when stressed, the holding period before the unloading permit the development of this phenomenon in way to avoid the formation of the "nose" (in Figure 14 no nose formation can be noticed at the beginning of the unloading). As previously observed, the second hold segment does not influence the calculation of the mechanical properties. Anyway the evolution of the second holding phase indicates that the time dependent phenomenon are present also during the unloading phase.

The quantitative analysis of the curves is reported in Figure 15.

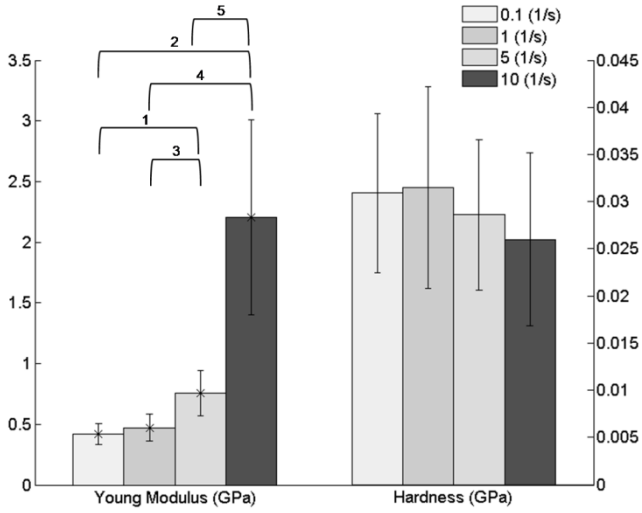

Figure 15: Left side: Average values of Young's modulus calculated for four different values of unloading rate. Right side: Average values of hardness calculated for four different values of loading rate. Statistical significant differences between mechanical characteristics and strain rate are reported. The bars indicate the statistical influence of the loading/unloading rate and the p-values ($1 - 1.21292 \cdot 10^{-13}$; $2 – 4.77149 \cdot 10^{-20}$; $3 – 2.12787 \cdot 10^{-10}$; $4 – 9.65004 \cdot 10^{-20}$; $5 – 3.46115 \cdot 10^{-14}$) calculated by using the ANOVA analysis with a confidence interval of the 95%

The values here presented of Young's modulus and hardness indicate a drastic reduction of the resistance to the penetration (reduced values of hardness) and an higher deformability of

the composite, due to the reduction of the Young's modulus, with respect the Harvard cement.

The ANOVA analysis shows a clear dependence of the elastic characteristics with the unloading rate, i.e. the Young's modulus values obtained for strain rate higher than $0.1\,s^{-1}$ are significant different. On the contrary, as for the Harvard cement, the hardness is not influenced by the selected values of strain rate and so by the loading/unloading values.

As noticed for the Harvard cement and highlighted by the ANOVA analysis, the first holding segment permit the development of the plastic time dependent phenomenon (Oliver & Pharr, 1992) since a constant values of hardness is obtained. As argued above, also for this composite, the length of the hold segment depends upon the primary creep rate that is proportional to the stress field generated during the first stage of the test (Whittaker, Harrison, Deen, Rae, & Williams, 2017).

Plot of the Young's modulus versus the chosen strain rate values (Figure 16) indicates an exponential relation between the two parameters. The value of R^2 equal to 0.9902 indicates

the strong dependence of the elastic characteristics by the duration of the unloading phase.

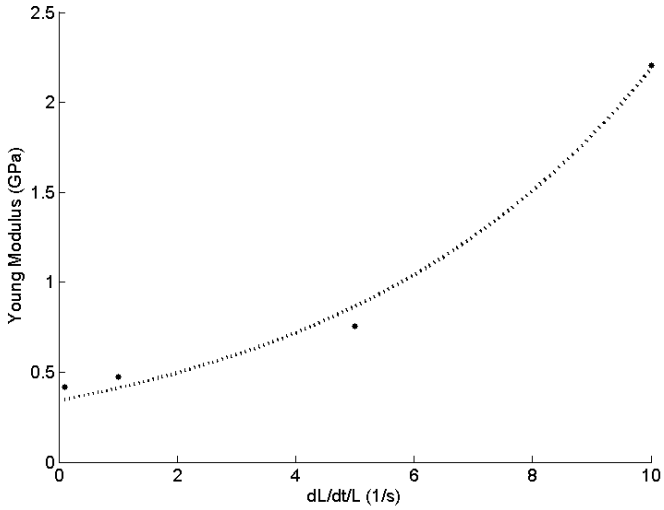

Figure 16: Black dots represent the mean value of the Young's modulus; dotted line represents the fitting exponential model

As noticed by Oliver and Pharr (Oliver & Pharr, 1992) the first part of the unloading curve is influenced by time dependent phenomenon that alter the shape of the unloading curves, furthermore other works have demonstrated that the stress field developed during the loading phase can contribute to alter the shape of the unloading curve. The higher intensity of the stress field underneath the tip could induce a changing of the polymer network, that influences the mechanical behavior of the cement during the unloading (Chang &

Zhang, 2009),(Vladislav, Gogotsi, & Dub, 2000), (Schuh, 2006). The combination of these two effects that are stress field dependent introduce a not negligible variability of the Young's modulus when the loading/unloading rate change (the stress field depends upon the loading rate imposed).

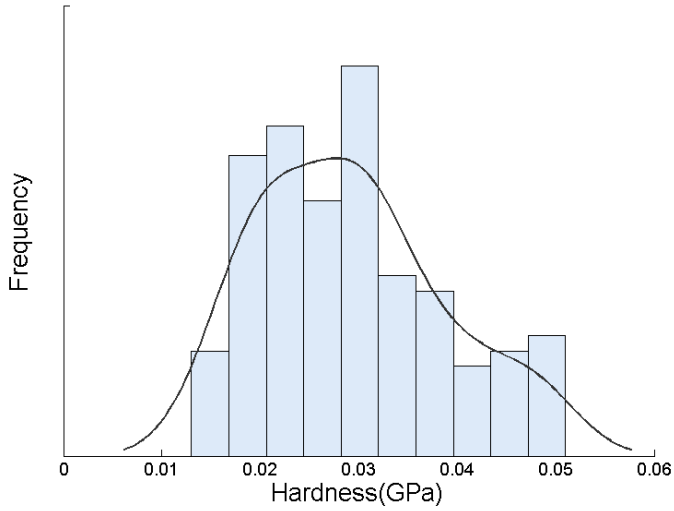

Figure 17: Histograms and probably density function (solid line) of hardness obtained for four values of stain rate. A- $0.1\left(1/s\right)$;B- $1\left(1/s\right)$; C- $5\left(1/s\right)$; D- $10\left(1/s\right)$.

The distribution of hardness values in a specific area of the sample gives an indication on how the phases of the composite are dispersed. In this case the histogram in Figure 17 is obtained combining the indentations performed in four different areas of the sample. Even if the indentation tests

were performed by imposing four different values of strain rate, the statistical analysis ensures that the strain rate does not influence the calculation of the hardness so the combination of all the tests is permitted. The histogram gives an indication on how the phases of the composite are dispersed. The distribution of the hardness values follows the PDF that is asymmetric, the presence of a peak at low values of hardness indicates that bismethacrilate and fillers, that compose the cement in equal parts, have the same mean value of hardness. The right tail of the PDF is due to the presence in low percentage of other phases.

Temp Bond

Same method was applied to the Temp Bond cement, in the Figure 18 four representative curves for the four values of strain rate are reported. The curves here reported clearly show a different behavior of this composite respect the previous ones. The loading/unloading curves, that characterize the response of the cement when stressed, is very close to that obtained for the other two composites; in this case, however a sharp division of the curves is evident when the strain rate

increases. For values of strain rate higher than 1 s^{-1} the composite shows an higher resistance to the penetration, indeed the maximum value of indentation depth decreases. Observing the holding phase, instead, comes out that the reached value of indentation depth is very close for the last two values of strain rate, indicating that a further increase of loading rate over the value of $5\,s^{-1}$ does not influence the evaluation of the hardness values.

The stiffening of the cement for increasing values of strain rate is found also in this case, therefore it can be concluded that this cement shows a viscoelastoplastic behavior.

Also for the Temp Bond a direct correlation between the strain rate and the creep rate can be observed, mostly during the primary creep. As a matter of fact the length of the holding step increases with the strain rate especially when the strain rate value pass from 0.1 to 1 s^{-1}. The relation between the strain rate and the length of the holding step in this case is not proportional, as a matter of fact the primary creep rate does not vary so much for values of loading rate higher than $1s^{-1}$.

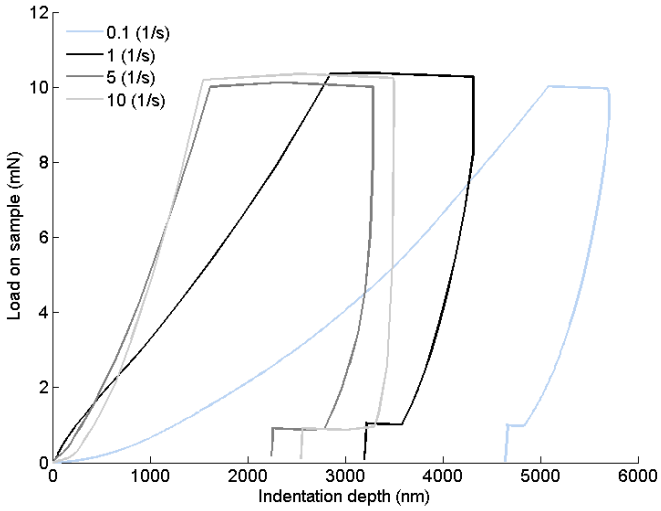

Figure 18: Representative curves of static test performed on Temp Bond cement, selecting 4 different value of loading/unloading rate

As for the previous tests, also, in this case the hold period last enough for avoid the formation of the "nose" in the first stage of the unloading rate, even if the time dependent phenomenon are present during the unloading phase as detected for the other two cements.

The evaluation of the Young's modulus and of the hardness is reported in Figure 19.

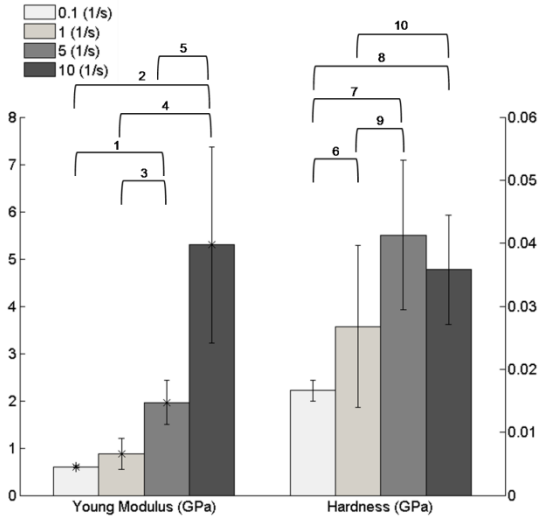

Figure 19 Left side: Average values of Young's modulus calculated for four different values of unloading rate. Right side: Average values of hardness calculated for four different values of loading rate. Statistical significant differences between mechanical characteristics and loading/unloading rate are reported. The bars indicate the statistical influence of the strain rate and the p-values (1 – $2.5972910 \cdot 10^{-16}$; 2 – $4.26037 \cdot 10^{-12}$; 3 – $7.72781 \cdot 10^{-16}$; 4 – $5.70284 \cdot 10^{-17}$; 5 – $3.33957 \cdot 10^{-12}$; 6 – 0.0017; 7 – $2.1354510 \cdot 10^{-11}$; 8 – $1.1454970 \cdot 10^{-5}$; 10 – 0.0033) calculated by using the ANOVA analysis with a confidence interval of the 95%

In this case the viscous characteristics of the composite influence also the hardness values. The reason have to be found in the creep rate that is correlated to the stress field underneath the tip as argued above. The stress field and so the dislocations movement, that determine the creep rate, develops in a way that make the evaluation of the hardness

instable. In this case the relation between the stress field and the primary creep rate changes if compared with the other two cements, a constant values of the primary creep rate is detected for strain rate values higher than 1 s^{-1}. In other words the creep rate is sensitive to the modification of the stress field only for values of strain rate below 5 s^{-1}.

The elastic response of the sample is governed by the same mechanisms observed for the Harvard and Temp Bond cements. The high intensity of the stress field under the tip(Chang & Zhang, 2009), (Vladislav, Gogotsi, & Dub, 2000),(Schuh, 2006), and the creep of the material during the unloading phase (Oliver & Pharr, 1992) are the major phenomena that characterize the unloading phase and so the elastic characteristics of the sample. Here, as for the previous cases studied, the different values of strain rate imposed, play a crucial role during the development of the stress field under the tip.

The elastic response of the composite is consistent with the results found for the other two cements. As a matter of fact the relation in Figure 19, confirms the non linear dependence of the Young's modulus by the loading rate.

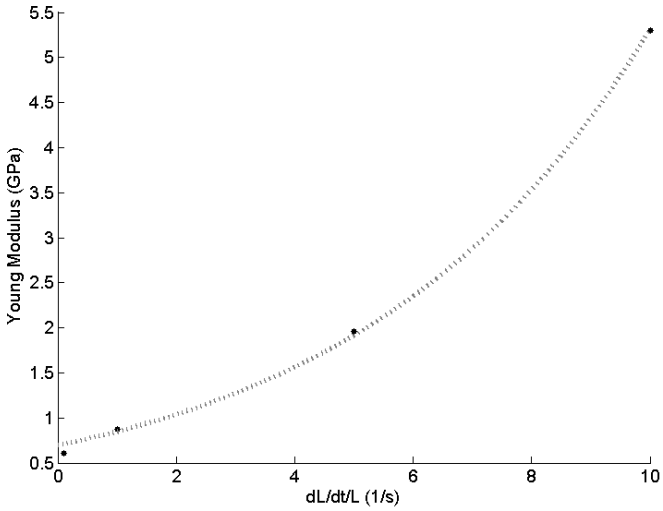

Figure 20: Black dots represent the mean value of the Young's modulus; dotted line represents the fitting exponential model.

The values of hardness reported in the histogram below, and the statistical analysis strengthen the proposed hypothesis of the dependence of the hardness by the strain rate, indeed the hardness values are significant different for strain rate values below to 5 s^{-1}.

In this case the analysis of the dispersion of the phases that compose the cement by using the hardness values cannot be applied. hardness results to be strain rate dependent. As a matter of fact the producer declares that the cement is

composed for the 95% of Zinc Oxide, but observing the histograms in Figure, in particular that obtained for strain rate values of 1and,10 s^{-1}, comes out the incoherency of using the distribution of the hardness values for determine how the single phases are distributed.

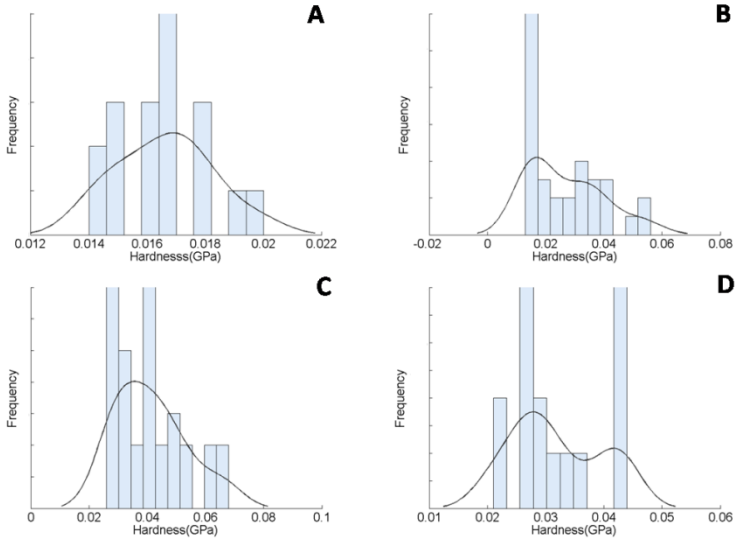

Figure 21: Histograms and probably density function (solid line) of hardness obtained for four values of stain rate. A- $0.1\,(1/s)$;B- $1\,(1/s)$; C- $5\,(1/s)$; D- $10\,(1/s)$.

As general behavior it was found that when the strain rate, imposed during the unloading stage, rises (and the unloading rate as a consequence rises) the coefficient *m* of the relation (1.16) assumes values even more high, introducing not

negligible errors on the calculation of the unloading stiffness and so on the evaluation of the Young's modulus.

1.3.2 Viscous elastoplastic (VEP) model

The results above presented, highlight the time dependence of the mechanical properties of the composites. As many works report, a way to reduce the time-dependent phenomenon is to introduce a hold phase before the unloading stage. Analysis of the curves indicates that the time-dependent phenomenon develop in a different manner when the loading unloading rate change. A Burges model (a Maxwell model in series with a Voigt model) has been applied to the first hold period registered during all static tests effectuated.

The creep displacement indicated in the graphs below is relative only to the holding phase. The creep displacement curves are characterized by three typical zone. The first one is known as transient creep or primary creep , the zone where the creep rate become constant is named steady-state creep or secondary creep and, the last one is the tertiary creep. For this study only the first two parts of the creep are taken into account.

Analyzing the unloading curves through the Oliver and Pharr method (results presented in the static test section) comes out that the viscosity of the material does not permit a reliable evaluation of the parameters, even if an hold segment is introduced before the unloading stage. In the light of that could be supposed that an incorrect evaluation of the Young's modulus is not due only to the shape of the unloading curve, but also to the phenomenon that take place during the holding stage (transient and steady-state creep). These types of composites are characterized by an elastic recovery that strongly depends by the loading history.

Harvard

The figure below, that shows the relation between the displacement registered during the first hold segment and the time explains the good agreement between the model and the experimental data.

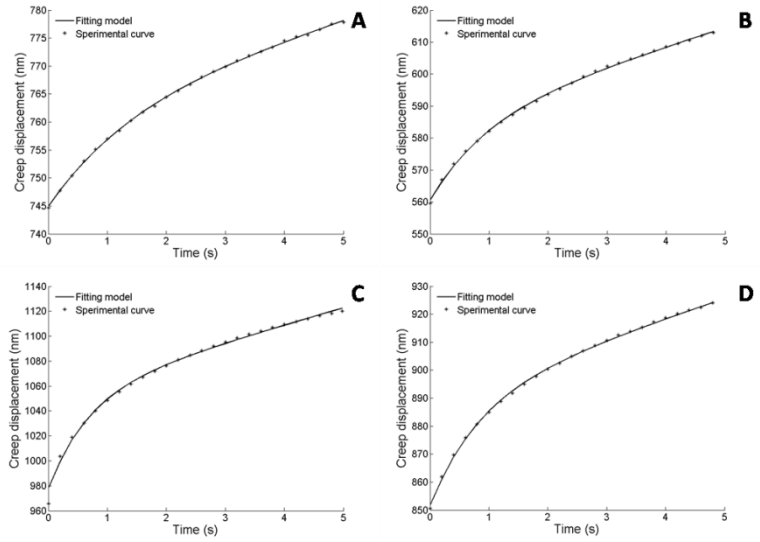

Figure 22 Creep displacement-time curves for the different values of loading rate, calculated on Harvard cement.

The experimental curves here reported are characterized by a first phase of transient creep, and a second phase (steady-state creep) where the creep displacement rate become constant, as a matter of fact the duration of holding time permit to achieve a constant creep displacement rate (data not shown).

During the steady-state creep the values of the strain rate has been calculated for the four different settings. The strain rate mean values (±standard deviation) calculated during the final stage of the holding segment are 0.0056(±0.0032), 0.0072(±0.0057), 0.0085(±0.0025), 0.0084(±0.0022) (s^{-1}) respectively, for strain rate values equal to 0,1 1 5 10 (s^{-1})

imposed during the loading stage. Statistical analysis indicates that the strain rate evaluated during the steady creep is in general stable, statistical differences were observed comparing the values obtained for 0.1 s^{-1} and 5 s^{-1} and between the values obtained for 0.1 s^{-1} and 10 s^{-1}.

Since the transient zone of creep displacement is strictly correlated to the visco-elastic phenomenon, variations of loading rate influence the creep during this first stage (Chien-Chao, Mao-Kuo, & Sanboh, 2011), without affect however the creep rate during the secondary creep. In other words the holding time is sufficient to avoid the formation of the nose as noticed before.

As reported in the work of Liu et al.(Liu & Lee, 2006) the Kelvin-Voigt elements of the Burgers model characterize the properties of the bulk material; and the surface properties of the sample are taken into account by the Maxwell system. In the Table 1 the values of the fitting parameters obtained with the Burgers model are reported. The parameters with the subscript 1 are inherent to the Maxwell model and the parameters with the subscript 2 label the parameters of the Kelvin-Voigt model.

Table 1 Fitting parameters for Harvard cement using flour different values of strain rate. The values that shear the same symbol are statistical different.

Strain Rate (s^{-1})	$\eta_{Q1}\left(Pas^2\right)$	$E_1\left(GPa\right)$	$\eta_{Q2}\left(Pas^2\right)$	$E_2\left(GPa\right)$
0.1	$9.3(\pm4.1)\cdot10^{13}$	$2.93(\pm0.82)$	$8.2(\pm4.8)\cdot10^{12}$	$5000(\pm2100)$
1	$5.0(\pm1.4)\cdot10^{13}$	$4.16(\pm1.78)$	$2.4(\pm1.1)\cdot10^{12}$	$3000(\pm1100)$
5	$2.1(\pm0.8)\cdot10^{13}$	$4.42(\pm1.67)$	$1.9(\pm1.7)\cdot10^{11}$	$748.5(\pm380.1)$
10	$3.8(\pm1.2)\cdot10^{13}$	$4.08(\pm1.60)$	$1.4(\pm0.6)\cdot10^{12}$	$1500(\pm541.2)$

The statistical analysis revealed that all the parameters obtained for strain rate values of 0.1 s^{-1} are significant different from that obtained for the other loading conditions, i.e. value of strain rate equal to 0.1 s^{-1} violate the hypothesis of instantaneous loading.

The order of magnitude of the viscosity parameters are coherent with the values found in literature (Oyen & Cook, 2003), (Marezan, Beyaoui, Bigerelle, & Guigon, 2012). During the holding period these two elements intervene in two different moment: the viscosity parameter of the Maxwell part

contributes to the steady-state creep; on the other side the second viscosity parameter combined with the second elastic element govern the transient creep. The comparability of these values indicates that are the elastic components that govern the model behavior.

As regards the elastic parameters, the value of E_1 does not change for strain rate higher than 0.1 $s^{-1}$and comparing the magnitude of the two elastic parameters is clear that the first one prescribes the model response. The very high values of the E_2 parameter is due to intrinsic characteristics of the nanoindentation test that generate a very high and local stress filed. Finally can be stated that the effective value of the Young's modulus of the composite is the value represented by the parameter E_1.

Telio CS Link

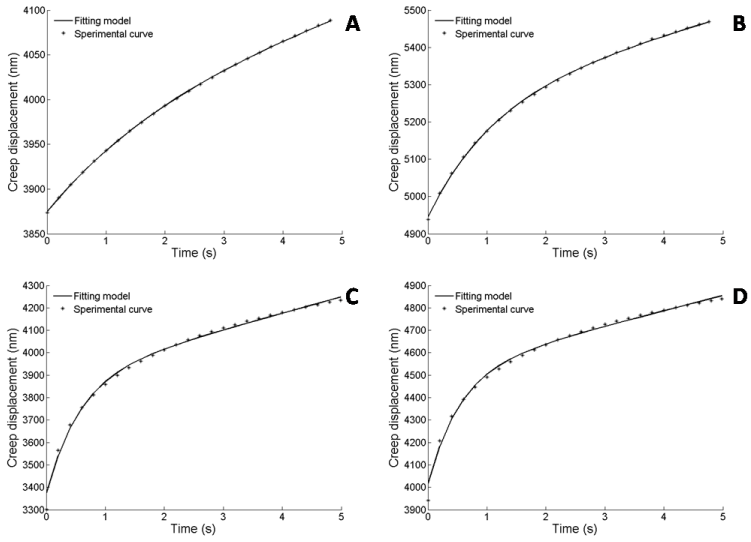

Figure 23: Creep displacement-time curves for the different values of loading rate, calculated on Telio CS cement. The values of the RMSE have been calculated:

Figure 23 reveals the good agreement between the model and the experimental data. As discussed above, also for the experimental curves here reported. Two typical creep segment can be recognized: a first non-linear zone that is the transient creep and, a second section where the creep become linear and the creep rate constant, known as steady-state creep.

Strain rate values have been calculated during the last stage of the steady-state creep, where the time dependent phenomenon are stable and the creep rate is constant. The strain rate mean values (± standard deviation) obtained are 0.0071(±0.0012), 0.0109(±0.0020), 0.0112(±0.0018), 0.0117(±0.0019) s^{-1}, respectively for the following strain rate values 0,1 1 5 10 (s^{-1}) imposed during the loading phase. Observing the graphs in Figure 23 the primary creep rate progressively increases when the strain rate imposed during the loading phase rise; in other words the creep rate that characterize the transient creep depends on the loading rate. In agreement with the results in literature (Chien-Chao, Mao-Kuo, & Sanboh, 2011). Conversely the strain rate calculated during the steady creep is not significant different when the imposed strain rate is higher than 0.1 s^{-1}.

The model parameters are reported in the table below.

The values of viscosity parameters are comparable with that found in literature (Chien-Kuo, Sanboh, Li-Piin, & N, 2006), (Marezan, Beyaoui, Bigerelle, & Guigon, 2012) for strain rate imposed values higher than 1 (s-1). Values of strain rate lower than 1 (s-1) violate the hypothesis made for solving the model, indeed give back not reliable parameters, as a matter

of fact the statistical analysis of the model parameters highlights that stable values of them are obtained when the strain rate values imposed during the loading are higher than 1 (s-1).

Table 2: Fitting parameters for Telio CS cement using flour different values of strain rate. The values that shear the same symbol are statistical different.

Strain Rate (s^{-1})	$\eta_{Q1}\left(Pas^2\right)$	$E_1\left(GPa\right)$	$\eta_{Q2}\left(Pas^2\right)$	$E_2\left(GPa\right)$
0.1	$7.2(\pm9.1)\cdot10^{12}$	$0.13(\pm0.032)$	$5.58(\pm1.79)\cdot10^{11}$	$130.68(\pm62.44)$
1	$8.94(\pm30.19)\cdot10^{16}$	$0.18(\pm0.063)$	$3.86(\pm1.22)\cdot10^{10}$	$21.55(\pm9.99)$
5	$5.32(\pm1.66)\cdot10^{11}$	$0.22(\pm0.067)$	$3.03(\pm1.26)\cdot10^{9}$	$10.23(\pm3.38)$
10	$6.18(\pm1.71)\cdot10^{11}$	$0.22(\pm0.087)$	$7.37(\pm5.74)\cdot10^{9}$	$13.97(\pm5.90)$

The two parameters intervene in different moment during the creep: the first viscosity parameter contributes to the steady-state creep, and the second one combined with the second elastic element govern the transient creep. The fact that the values of η_{Q2} are lower that the values obtained for η_{Q1}

confirms that the creep rate during the transient creep is higher than that registered during the steady creep. For this composite the elastic and viscous elements equally contribute to dictate the model behavior.

As regard the values of Young's modulus the contribution of the parameter E_1 dominates the elastic response of the model, and as argued above indicates the surface properties of the sample, indeed its values are comparable with the experimental one. The reduced stiffness of this composite is highlighted by the values of the E_2 that are very lower if compared with that obtained for the Harvard cement.

The results here presented confirm that the setting of the loading rate is crucial for the correct evaluation of the Young's modulus, when model of such type are applied.

Temp Bond

Also in this case the model is able to fit the experimental curves (see Figure 24).

The experimental curves are characterized by a first phase of transient creep and a second phase of steady-state creep, as a matter of fact the creep rate after a transient period reach a

constant value in correspondence of the steady-state creep, i.e. the strain rate values calculated during the last stage of the steady-state creep (0.0015(±0.0012), 0.0020(±0.0028), 0.0018(±0.0034), 0.0019(±0.0010) respectively, for the following values of strain rate 0,1 1 5 10 (s^{-1}) imposed during the loading phase) do not show statistical differences.

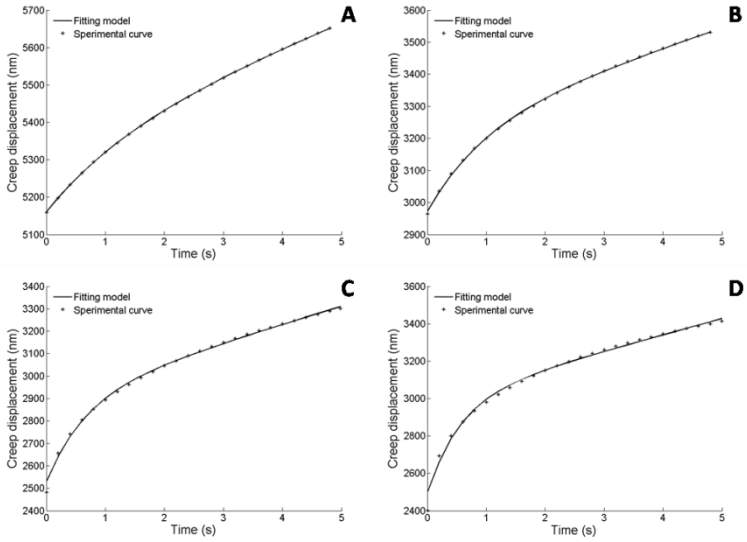

Figure 24*:* Creep displacement-time curves for the different values of loading rate, calculated on Telio CS cement. The values of the RMSE have been calculated.

The behavior of this cement during the holding phase is very close to that of the Telio CS composite: the strain rate values

and the creep displacement evolve in the same manner. The values of the model parameters are reported in Table 3.

Table 3*:* Fitting parameters for Telio CS cement using flour different values of strain rate. The values that shear the same symbol are statistical different.

Strain Rate (s^{-1})	$\eta_{Q1}\left(Pas^2\right)$	$E_1\left(GPa\right)$	$\eta_{Q2}\left(Pas^2\right)$	$E_2\left(GPa\right)$
0.1	$5.12(\pm0.88)\cdot10^{11}$	$0.10(\pm0.0093)^{*\circ}$	$1.66(\pm0.26)\cdot10^{11*\circ\cdot}$	$38.81(\pm9.75)^{*\circ}$
1	$1(\pm2.87)\cdot10^{13}$	$0.22(\pm0.098)^{***}$	$2.35(\pm1.37)\cdot10^{10***}$	$12.9(\pm7.95)^{*}$
5	$3.57(\pm0.84)\cdot10^{11}$	$0.44(\pm0.18)^{\circ**}$	$4.14(\pm1.70)\cdot10^{9\circ**}$	$11.81(\pm3.45)^{\circ}$
10	$4.22(\pm1.29)\cdot10^{11}$	$0.40(\pm0.11)^{\cdot\circ\circ}$	$1.02(\pm0.95)\cdot10^{10\cdot}$	$16.82(\pm8.52)^{\cdot}$

The order of magnitude of the reported values is comparable with that found in literature when the strain rate imposed is higher than 1 s^{-1}. Also in this case the value of the viscous parameters indicates that during the primary creep the time dependent phenomenon develop faster than that registered during the steady state creep.

Also in this case the contribution of the parameter E_1 dominates the elastic response of the model, and representing the surface properties of the sample, its values can be compared with the experimental one. The reduced stiffness of this composite is highlighted by the values of the E_2 that are very lower if compared with that obtained for the Harvard cement.

The results here presented confirm that the setting of the loading rate is crucial for the correct evaluation of the Young's modulus, when model of such type are applied.

1.3.3 Quasi-static tests

Static tests and the model have highlighted the crucial role of the strain rate values set during the loading phase. Quasi-static tests allows to achieve a deeper understanding of how this factors influence the unloading process.

The results obtained for all the analyzed composite indicates that the unloading rate is the main parameter that effect the results of the test, in other words the Young's modulus value is strictly related to the unloading rate. The method here

applied, however, suggests that the elastic response of the materials could be correctly evaluated if the real value of the strain rate is used. As a matter of fact even if four different values of loading rate have been set in four different batch of 20 tests, the values of Young's modulus obtained seems to be stable. The method here adopted make the evaluation of the elastic properties independent by the value of the loading/unloading rate chosen.

It is necessary to keep in mind that, in accordance with the relation defined in the chapter dedicated to the indentation theory and reported below:

$$S = \frac{2}{\sqrt{\pi}} E_r \sqrt{A}$$

the Young's modulus can be considered uniform along the thickness of the sample, if the relation between the unloading stiffness and the indentation depth is linear.

The reduction of the Young's modulus with the progression of the test and so, with the reduction of the time dependent phenomenon (proven by the reduced length of the hold period set during the unloading phase) confirm that the viscous characteristics of these cements introduce an overestimation

of the Young's modulus, when evaluated with a typical nanoindentation protocol of static test. Phenomenon already observed during the static tests.

As found in literature, similar tests conducted on viscoelastic materials indicate that the Young's modulus decrease with the increasing of the indentation depth and reaches a plateau where the value can be considered reliable (Briscoe, Fiori, & Pelillo, 1998).

Harvard

Quasi-static tests performed on the Harvard cement for four different values of strain rate are shown in Figure 25 (one representative test has been chosen). As observed for the static experiments and elsewhere (Zhang, Shao, Li, & Jiang, 2016) for increasing values of the imposed strain rate, the creep rate rises, and as a consequence the length of the hold segment, registered during the cycles, grows.

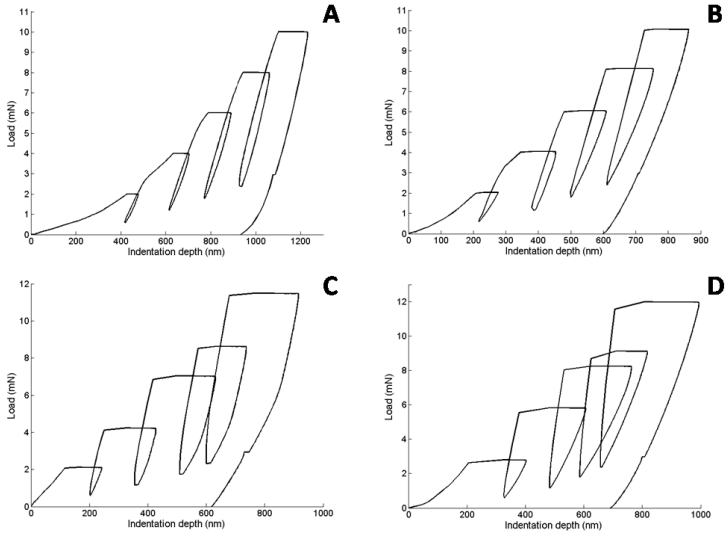

Figure 25: Representative curves of quasi-static test performed on Harvard cement, selecting 4 different value of loading rate: (A) -$0.1\,(1/s)$; (B) -$1\,(1/s)$; (C) -$5\,(1/s)$; (D) -$10\,(1/s)$

As noticed above and by Whittaker et al. (Whittaker, Harrison, Deen, Rae, & Williams, 2017) the correlation between the stress field and the creep rate does not change during the experiment here reported: when the loading rate rises the indentation depth reached for every cycle decrease even if the load is fixed. In other words when the loading rate rises the same load is distributed on a reduced surface, indeed the stress field increases and, consequently the displacement of the indenter become even more faster. The progressive

overlapping of the cycles is due to the higher values of loading rate respect the unloading rate. During the loading phase the strain rate values for each cycle of the test is constant, the unloading rate instead, is calculated by evaluating the strain rate during the hold segment. During the unloading phase of the last cycle of the tests reported in Figure 25 a reduction of the time dependent phenomenon can be observed if compared with the analogous static tests. The displacement registered during the second holding phase of the unloading step of the last cycle is dramatically reduced if compared with the static tests.

The curves here analyzed are characterized by five cycles, for every cycle the Oliver and Pharr method can be applied an so five values of unloading stiffness, indeed of Young's modulus, can be calculated at different indentation depth; in correspondence of every unloading step.

In Figure 26 is reported the plot between the indentation depth and the unloading stiffness, calculated during the unloading step of every cycle for all quasi-static tests performed on the Harvard cement.

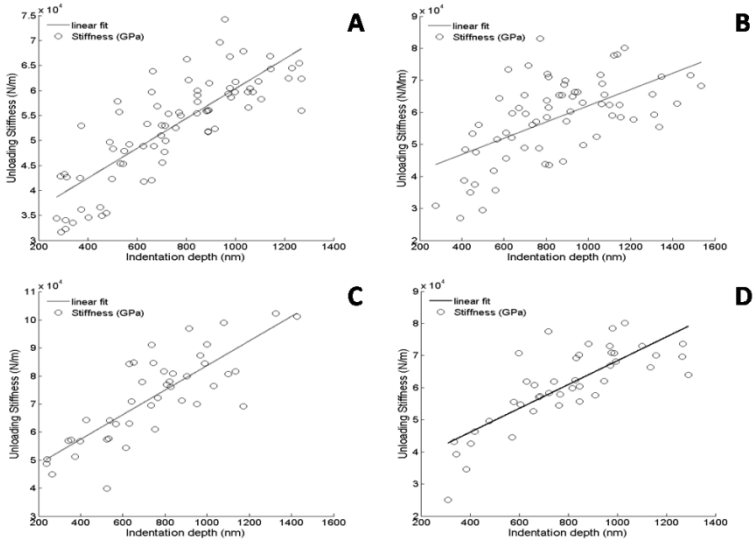

Figure 26*Figure* Relation between the unloading Stiffness and Indentation Depth calculated for every cycles of all test performed on Harvard cement

Due to the high dispersion of the unloading stiffness values for increasing values of indentation depth, shown in Figure 26 seems not follow a perfectly linear relation. Unhomogeneity of the sample, highlighted by the static analysis, address the dispersion of the data in Figure 26 to the chosen location for performing the indentation, on the other side the unhomogeneity along the thickness of the sample is due to the time dependent phenomenon that make the relation reported above not true.

As proven by the data shown in the Figure 27 where the relation between the Young's modulus and the indentation depth for different values of loading rate is reported.

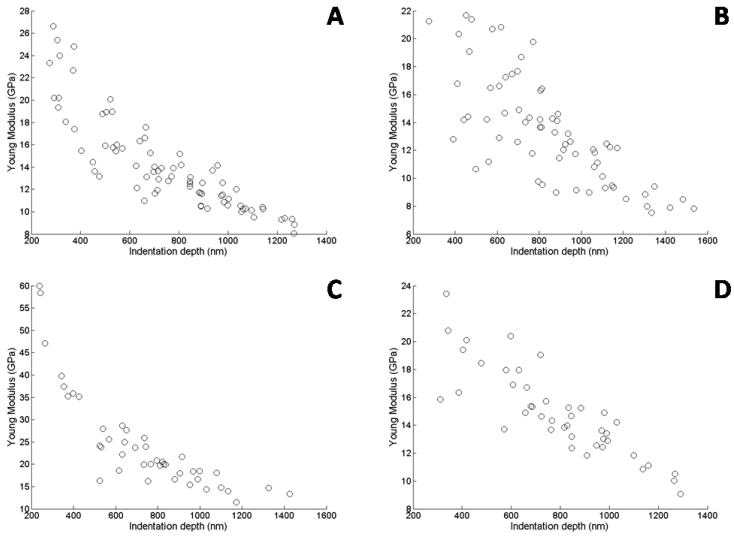

Figure 27*Figure* Relation between the Young's modulus and Indentation Depth calculated for every cycles of all test performed on Harvard cement.

The unloading rate, differently from the static test, has been calculated by evaluating the strain rate during the hold period imposed before the unloading step of every cycle; as general trend a decrease of the modulus values is observed. Even if the starting values of the Young's modulus changes with the loading rate imposed (variability due to the intrinsic

heterogeneity of the sample (Briscoe, Fiori, & Pelillo, 1998)), the values obtained for increasing depth tend to stabilize for all the loading rate values chosen, during the last cycle. The stabilization of the Young's modulus values indicates that the time dependent phenomenon do not influence the unloading curves, as proven by the reduction of the length of the second holding time (Figure 25) if the correct values of strain rate is chosen. It is fundamental to note that here only the effect of time dependent phenomenon have been analyzed, and not the elastic response of the elements that compose the cement. In other words here no information on the single phases of the composite have been given.

Telio CS Link

The figure below shows the load-displacement curves obtained for quasi-static test performed on the Telio CS cement.

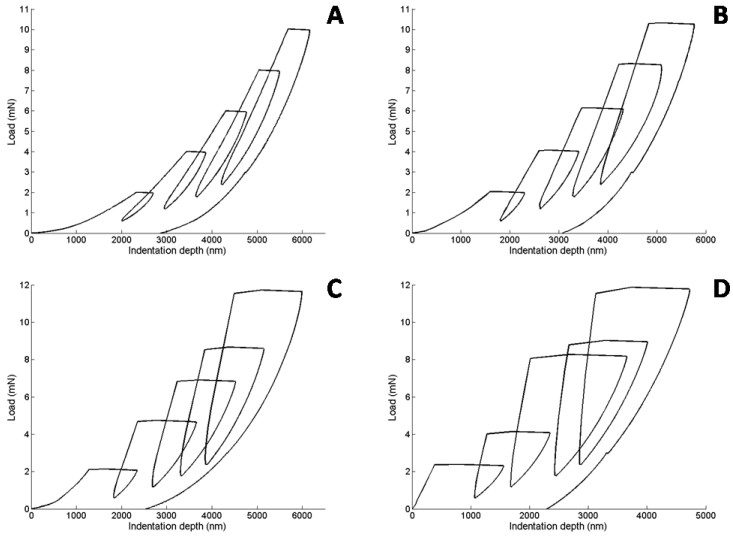

Figure 28: Representative curves of quasi-static test performed on Telio CS cement, selecting 4 different value of loading rate: (A) - $0.1\,(1/s)$; (B) -$1\,(1/s)$; (C) -$5\,(1/s)$; (D) -$10\,(1/s)$

The effect of progressive increase of the loading rate on the creep rate is the same observed during the static tests: the length of the hold segment increases with the loading rate. The increasing of the stress field is reflected in an increase of the creep rate(Whittaker, Harrison, Deen, Rae, & Williams, 2017). The indentation depth reached before the hold phase, during the cycles, decreases for increasing values of the strain rate but the load does not change, consequently the stress field increases.

Overlapping of the curves become even more evident for increasing values of the strain rate, phenomenon formerly observed during the tests made on the Harvard cement. As noticed above the overlapping is due to the increasing difference between the loading rate of the successive cycle and the unloading rate of the previous one.

The method here applied permit to reduce considerably the time dependent phenomenon during the unloading phase of the last cycle, as a matter of fact the second hold period (hold segment imposed during the last unloading step), if compared with the analogous obtained during the static tests, results to be dramatically decreased.

Finally can be concluded that also for this type of composite the time dependent phenomenon reduces and a better estimation of the Young's modulus is achieved. The method here applied, furthermore, permits to calculate the mechanical properties along the thickness: since, for every cycle, a value of unloading stiffness can be calculated in correspondence of a well defined value of indentation depth. The figure below shows the values of unloading stiffness calculated imposing four different values of strain rate.

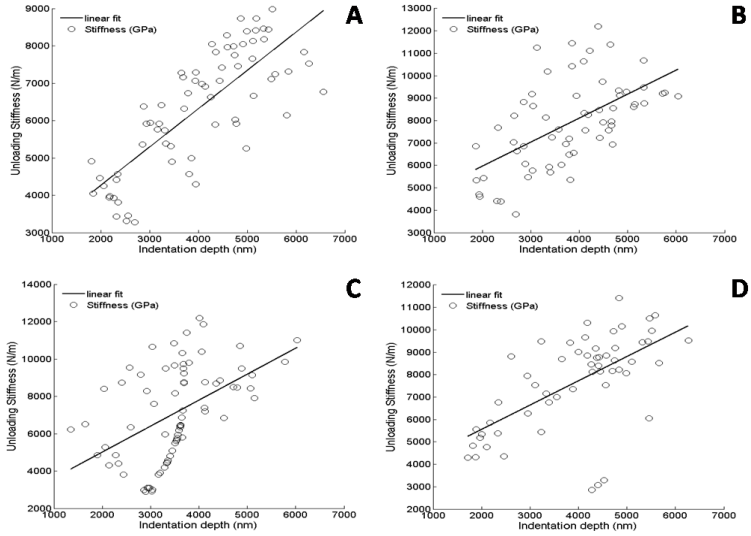

Figure 29*Figure* Relation between the unloading Stiffness and Indentation Depth calculated for every cycles of all test performed on Telio CS cement.

The relation between the unloading stiffness and the indentation depth, as a general trend seems to be linear. The low values of the R^2 parameter is due to the high dispersion of the unloading stiffness. For homogeneous materials if there is a linear relation between the unloading stiffness and the indentation depth the values of the Young's modulus must be constant.

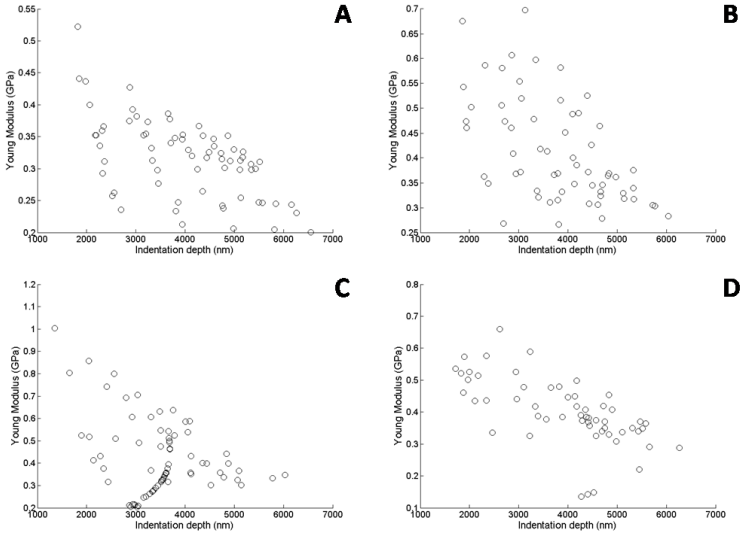

Figure 30: Relation between the Young's modulus and Indentation Depth calculated for every cycles of all test performed on Telio CS cement.

Observing the trend in Figure 30, neither for this composite the relation between the elastic modulus and the unloading stiffness is true, as a matter of fact the sample results to be inhomogeneous, also along the thickness.

As observed for the Harvard cement the Young's modulus values obtained at shallows depth are characterized by an higher dispersion if compared with the values obtained for deepest indentation. Such dispersion that characterize the first cycle of the four types of tests is due to the time dependent

phenomenon, that diminish during the tests. The method here proposed permits to stabilize the Young's modulus values calculated, for the different values of strain rate impsed during the loading phase. As a matter of fact the time dependent phenomenon are almost inexistent. The impressive reduction of the hold segment registered during the unloading phase of the last cycle for all the types of tests (Figure 28) hints that the time dependent phenomenon do not influence the unload phase in a significant way.

Temp Bond

The last composite that has been undergone to the cyclic tests is the Temp Bond. The figure below shows the results.

Creep rate here registered seems to be slightly influenced by the different values of loading rate imposed: the hold segment length does not differ so much between the tests. The principle for which the creep rate increases with the stress field is valid (Whittaker, Harrison, Deen, Rae, & Williams, 2017), but as observed above and for static tests, the creep rate is less sensible to loading rate variation, as a matter of

fact also the stress field slightly change with the loading rate. Observing the tests in Figure 31 can be stated that during the unloading phase the deformation recovery is very low, indicating that plastic phenomenon dominates the response of the composite.

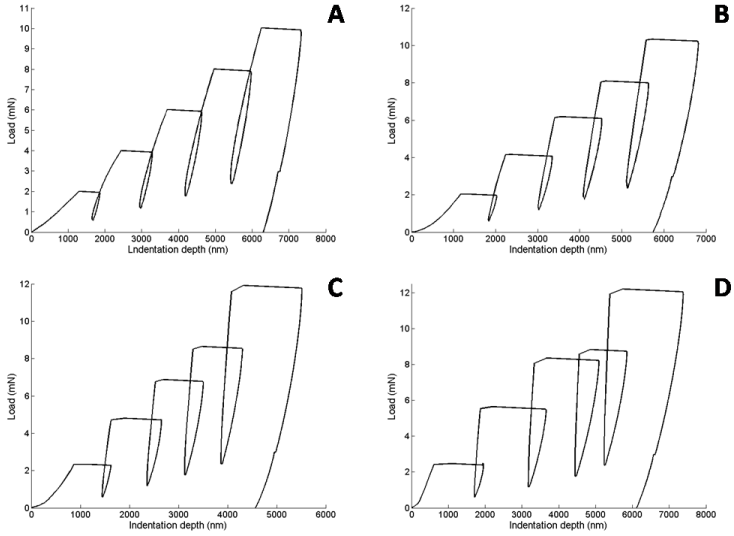

Figure 31*:* Representative curves of quasi-static test performed on Temp Bond cement, selecting 4 different value of loading rate: (A) - $0.1(1/s)$; (B) - $1(1/s)$; (C) - $5(1/s)$; (D) - $10(1/s)$.

In the light of the observations made above it can be stated that the time dependent phenomenon in this case slightly interfere with the response of the cement in particular during the unloading phase, i.e. if the creep rate moderately changes

when the loading/unloading rate change the time effect on the test is in the same way moderated.

A severe overlapping of the cycles is registered only for the tests performed for strain rate values higher than 1 s^{-1}. Analyzing the unloading curves in Figure 31 it can be stated that the method, developed in way to reduce the time dependent phenomenon during the unloading phase, works also for this composite: the length of the hold segment registered during the unloading phase is dramatically reduced respect the static tests.

The method, as formerly observed, allows to characterize the cement also along the thickness of the sample. Five values of Unloading Stiffness can be calculated in way to obtain five values of Young's modulus. Figure 32 shows the values of unloading stiffness calculated for the four values of strain rate. The reduced variability of the Unloading Stiffness values can be observed in the figure, and by observing the R^2 values it is clear that the relation of the unloading stiffness with the indentation depth is linear. The values of R^2 very close to one registered in this case respect the analysis conducted on the others two cements indicates that the variability of the evaluated mechanical characteristics is strongly affected by

the viscous related phenomenon that take place during the test.

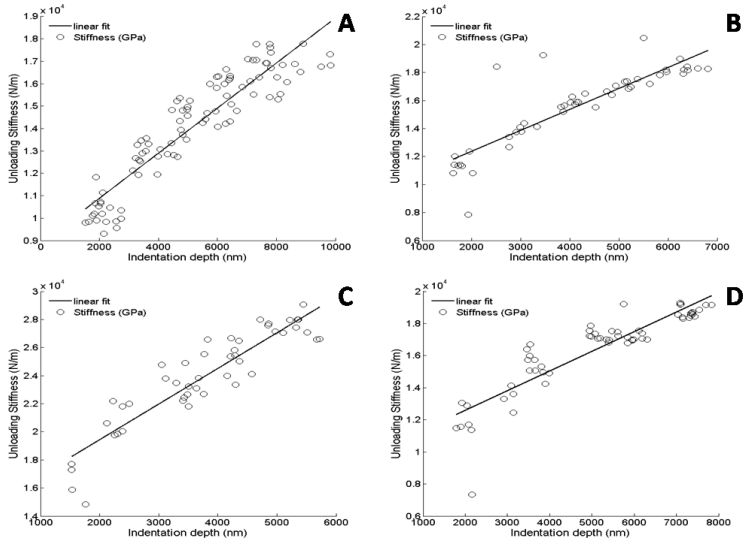

Figure 32: Relation between the unloading Stiffness and Indentation Depth calculated for every cycles of all test performed on Temp Bond cement.

The relation reported above indicates that the Young's modulus have to be constant, relation that is valid for homogeneous materials that do not show time dependent characteristics. The figure below reports the variation of the Young's modulus along the thickness of the sample.

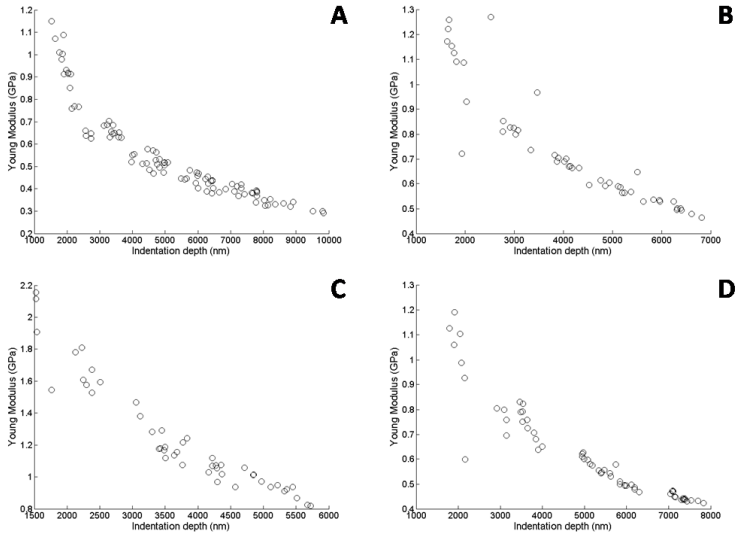

Figure 33: Relation between the Young's modulus and Indentation Depth calculated for every cycles of all test performed on Temp Bond cement.

As observed for the other two cements, the Young's modulus decreases along the thickness of the sample and for the higher values of the indentation depth (in correspondence of the last cycles), the modulus values tend to reach a stable values.

This type of cement is less affected by time dependent phenomenon and as a result the Young's modulus as such as the unloading stiffness is characterized by a reduced dispersion. Consequence of a reduced impact of the time dependent phenomenon on the evaluation of the elastic

characteristics, is that the Young's modulus reach a well defined stable values during the lasts cycle of indentation.

In the light of that can be stated that the values of modulus calculated with this method, indeed starting from curves obtained in condition of reduced time dependent phenomenon, could be considerate more accurate an nearest to the true values.

In the light of the results above presented it can be stated that using the wrong values of strain rate during the unloading phase, correspond to withdraw the tip at a rate that does not permit to record the actual displacement of the sample surface, in other words the displacement registered during the unloading phase is a counterfeit displacement.

The results obtained with this new method (Table 4) has been confronted with that obtained by applying a correction formula (Feng & Ngan, 2001) to the unloading stiffness calculated with the Oliver and Pharr method, reported below:

$$\frac{1}{S_e} = \frac{1}{S} - \frac{\dot{h}_u}{\dot{P}_u} \tag{1.38}$$

where the $\dot{h_u}$ is the time derivative of the displacement registered during the hold period and the $\dot{P_u}$ is the time derivative of the load during the unload.

Table 4: Comparision between the values of Young's modulus obtained using the new experimental method and the correction formulas.

	HARVARD (GPa)		TELIO CS LINK (GPa)		TEMP BOND (GPa)	
Strain rate (s^{-1})	*New method*	*Corrected value*	*New method*	*Corrected value*	*New method*	*Corrected value*
0.1	12.76(±5.3)	9.70(±3.1)	0.31(±0.1)	0.20(±0.1)	0.36(±0.1)	0.12(±0.010)
1	10,29(±2.8)	9.70(±3.2)	0.39(±0.1)	0.36(±0.1)	0.62(±0.2)	0.47(±0.19)
5	20.09(±5.1)	24.27(±5.3)	0.57(±0.1)	0.67(±0.1)	0.96(±0.1)	1.55(±0.33)
10	14.13(±2.5)	78.31(±21)	0.29(±0.1)	2.04(±0.7)	0.46(±0.1)	4.55(±1.73)

The Young's modulus values obtained with the two method are comparable only for the first two values of the strain rate imposed. The correction formula, works well when the time dependent phenomenon evolve slowly. Instead the values obtained with the application of the quasi static method seem to be less effected by the increasing of the strain rate. Finally it can be concluded that if the strain value imposed is kept

under a determined threshold the new approach can give reasonable results.

1.4 Conclusions and future works

Nanoindentation is a promising technique for the mechanical characterization of all kinds of materials. The relative simplicity of the sample preparation, the non-destructivity nature of the test and, the extended features of the sample that this technique permits to analyze pushed this technique to expand even more.

This type of analysis is based on the studies of the contact mechanics conducted, starting by the beginning of the past century, by Bussinesq, Love, Hertz and, Sneddon. The technological advances introduced by Doerner and Nix, Oliver and Pharr, Cheng and Cheng... bring this technique to spread out in the majority of the world laboratories for the mechanical characterization of the more disparate kinds of materials.

As usual the medal has two faces, if this technique is very promising and versatile for the relative simplicity of the execution of the test, the counter part is that the model on

which the method is founded work well for an elastic-half space. As well established do not exist materials that can be considered perfectly elastic or perfectly plastic or perfectly viscous, but usually, the materials response is held by a combination of these characteristics or some times, as in this study, by all the three aspects are present.

The studies conducted by Oliver and Pharr have shown that for elastoplastic materials, the data obtained, if well treated give reasonable results.

With the introduction of new and, even more complex materials that are required for the application of the new technologies that often go down until the nano-scale, this method has to deal with the viscous characteristics of these materials.

A lot of studies and conjecture have been developed in way to understand how the viscous phenomenon effect the curves obtained by the nanoindentation tests and what is the best method to identify and separate the phenomenon. On the basis of this studies and consideration, here a small contribution to the studies try to be given.

The approach used in this studies has shown that the information acquired during the hold period can be used to reduce the time-dependent phenomenon during the unloading phase in way to catch the only elastic response of the composites.

This is only the tip of the iceberg, and a lot of studies and experiments have to be performed. As well recognized in literature (Briscoe, Fiori, & Pelillo, 1998), (Tsui, Oliver, & Pharr, 1995), (Balshakov, Oliver, & Pharr, 1995) the results of a nanoindentation test are size effects dependent, i.e. the goodness of the mechanical characteristics evaluated are strictly related to the estimation of the contact area. The main effect of the viscous characteristics is on the evaluation of the displacement when a certain load is reached, which is reflected on the estimation of the contact area that depends on the penetration depth. In addition the data have to be evaluated also considering the phenomenon of the pile-up (the contact area of the indeintaiton is overestimated) and the sinking-in (the contact area is underestimated) (Oliver & Pharr, 2004), that can be evaluated only if an image of the imprint leave by the punch can be taken, in way to measure the real contact area. The possibility of a direct evaluation of

the real contact area did not be considered for the color of the cement surface and the characteristics surface roughness, but mostly for the time dependent phenomenon that are active also when the test is concluded, and a whole recovery of the deformation could occur. These aspects make the evaluation of the contact area impossible.

In the light of this consideration, a model like that used in this study, has been adopted trying not only to gain more information on the viscous properties of the materials during the creep but also to try to individuate a reliable model that can be used for a computer aided simulation of the indentation process. The simulation of the process could be clarify the effects of the viscous phenomenon on the evaluation of the real contact area.

Chapter 2

Nanoindentation Based Approach for the Mechanical Characterization of Polymeric Microspheres for Drug Delivery

Part of this chapter is published in the journal: Materials Science and Engineering C 75(2017) 408-417.

Author: Costantino Del Gaudio, Valentina Crognale, Gianpaolo Serino, Pierluca Galloni, Alberto Audenino, Domenico Ribatti, Umberto Morbiducci

2.1 Introduction

2.1.1 Use of drug delivery systems instead of traditional therapeutic systems

Development of targeted drug delivery systems (DDSs), has been fostered by a decline in the formulation of new drugs in the recent years (Ranade, V.V., & Cannon, third edition, 2011). Development of new drug molecules is expensive and time consuming indeed, the possibility to present the well known drugs in new forms, including novel delivery approaches to improve their safety-efficacy ratio (Tiwari, Tiwari, B., Pandey, & Saurabh, 2012 , 2 (1)) is an attractive solution. Drug delivery technology has not only benefited tens of millions of patients by relieving suffering and prolonging life, but they have also changed the economics of drug development (Zhang, Chan, & Leong, Advanced materials and processing for drug delivery: The past and the future, Advanced drug delivery reviews, 2013), as a matter of fact the average cost required to develop a new DDS (approximately $ 20-50 million and 3-4 years) is significantly lower than that required for a new drug molecule (approximately $ 500 million and over 10 years) (Sanjay, 2001). Roughly speaking,

drug delivery system are all that means that can bring the pharmacologically active molecule in the targeted district of the body, in order to maximize the affect of the drug with minimal side effect. The success of the application of such systems is strictly related to the quantities of the drug released in a determinate period of time.

Nowadays the majority of pharmaceutical formulations are systemically administered, therefore they have to overcome various biological barriers, such as organs, cells and even intracellular compartments, often causing undesirable side-reactions or being partially inactivated (Harsha, Chandramouli, & Rani, Ofloxacin targeting to lungs by way of microspheres, 2009).

When drugs are administered orally or injected, often at a site remote from the target tissue, there are other drawbacks, such as fluctuating drug levels in the body, that often imply (1) the administration of new and higher doses of drug, (2) poor drug efficacy, and (3) poor patient compliance (Edlund & Albertsson, 2002). These systems do not allow to control the concentration, duration and bioavailability of bioactive substances, thus limiting the expected therapeutic outcome.

In this regard, the development of targeted drug delivery systems represents a valuable option and a promising clinical treatment, at the same time. The proposed approach can improve the therapeutic efficacy, reduce adverse reactions, provide patience compliance and, most importantly, allow a controlled and localised delivery of drugs, reducing the total amount of drug required and maintaining a constant delivery of drugs over time. Such systems with reproducible and predictable release kinetics do not necessitate multiple administrations and a proper drug concentration can be provided to the target site. The major advantage introduced by the DDS is that the distribution of drug in the body depends on the physicochemical properties of the carrier and not on those of drugs (Harsha & Rani, 2006). The carrier contain the drugs that will not be delivered until the carrier will be at the target site (Petrak, 2005), i.e. the carrier is the barrier that divide the drug by the external world and prevent every kind of interaction with the physiological environment before the DDS reaches the target. The kinetic of the drug delivery can be manipulated by choosing an appropriate carrier, or by changing the physicochemical properties of the latter (Harsha & Rani, 2006).

Some factors could alter the action of pharmaceutical molecules: degradation, interaction with other cells and, incapacity to penetrate tissues (Vilar & Albericio, 2012). Therefore, drugs must be encapsulated for being protected against the external medium. Controlled release systems provide protection of drugs that would be otherwise rapidly destroyed by the body, protecting them from environmental hazards and from interacting with other molecules which could modify their chemical structure. Furthermore, DDSs can be regarded as a valuable means for the release of potentially toxic drugs, especially anticancer agents, that can be directly released in high concentrations to the tumor site, increasing the efficiency and minimizing systemic exposure and subsequent side effects (Edlund & Albertsson, 2002).

However, several issues need to be addressed when a drug has to be loaded into a DDS and subsequently released. One of the more important drug properties to be considered is its potency. As a general rule, the lower the drug content carried by a DDS, the more potent the drug must be in order to deliver a therapeutic concentration of drug. Drugs with higher potencies are needed in some types of DDSs which can carry only a few molecules of a drug, such as immunotoxins and immunoconjugates, or such as polymer conjugates, that can

carry tens of molecules. When a drug has been chosen, its chemical, physical and biological properties, such as stability, solubility, size, and possible electrical charge, should be understood and integrated into the choice of the carrier material. The materials challenge is matching drug properties to complementary carrier materials.

Other aspects to analyse are whether the drug will "survive" the procedure required for its incorporation into the DDS, and whether the carrier can help to stabilize the drug or prevent premature metabolic breakdown. Clearly the regulatory status of the drug may also play a role in the decision to use a particular DDS, in other words, if the free drug is already in clinical use, it is necessary to evaluate the advantages of the DDS compared to the free drug. Moreover, the mechanism of action of a drug may also dictate its suitability for delivery in a particular DDS (Allen & Cullis, 2008).

2.1.2 Drug delivery system: state of art

Most of the FDA approved DDSs are liposomes or lipid-based systems, which are mainly used for immunological and dermatological applications, vaccine adjuvant, eye disorders,

brain targeting, infective disease and tumor therapy (Samad, Sultana, & Aqil, 2007). Liposomes are spontaneously formed when phospholipids are dispersed in aqueous medium: the hydrophilic interaction of the lipid head groups with water, results in the formation of multi-lamellar and uni-lamellar systems (vesicles). Therefore, liposomes are spherical vesicles that consist of an aqueous compartment enclosed by a phospholipid bilayer. If multiple bilayers of lipids are formed around a primary core, the structures are called multilamellar vesicles.

Liposomes were recognized as models to study biological membranes and as versatile DDSs of both hydrophilic and lipophilic molecules.

The use of liposome-formulated drugs to treat cancer and systemic or local fungal infections is widely accepted, mainly because they are biologically inert and biocompatible (Schwendener, 2007).

Another strategy for molecularly targeted drug delivery is to use antibodies attached to liposomes (immunoliposomes), being non-immunogenic and capable of long circulation even with repeated administrations. The idea behind this

technology is to deliver potent drugs to the target site by using the specificity of monoclonal antibodies (mAb), thus avoiding non-targeted organs toxicity. By selecting the appropriate molecular domains, these systems can be used across a wide spectrum of diseases (Martinho, Damgé, & Reis, 2011).

Also viruses are potential vehicles for drug and gene therapies, due to their natural ability to infect specific cells and transport material to the nucleus.

Polymers have played an integral role in the advancement of drug delivery technology, because of the possibility to regulate the release profile of a polymeric-based DDS by varying their physical and chemical characteristics of the polymeric matrix (Dias & Hendriks, 2001).

Wichterle and Lim proposed the first polymeric DDS using the hydrogels in 1960. In 1966 Folkman and Long presented a new DDS based on the diffusion of small molecules through the wall of silicone.

Advances in the use of polymeric materials have been introduced with the discover of the polymeric-micelles the hydrophilic and hydrophobic monomers are capable to self

arrange in a shell-like structure like the micelles. The drug can be physically entrapped in the core of polymeric micelles.

Other aspects that make the use of polymer attractive is the possibility to create smart DDS, which are able to release the drug when an external stimuli is given, or change in local environment (Zhang, Ouyang, Lim, Ramakrishna, & Huang, 2005).

2.1.3 Biocompatibility and biodegradability

The prerogative of a material that have to be used for medical application is the biocompatibility, that is the capability of the material to non elicit immunological, toxic or injurious effects, when introduced in the biological environment(Edlund & Albertsson, 2002).

The biodegradability and bioresorption in the biological environment is the main characteristics of a microsphere or, in general, of a DDS. The degradation process of the polymer that constitutes the device trigger the rate of the drug diffusion (Hamdi, Ponchel, & Duchene, 1998). To overcome every ambiguity Vert (Vert, Bioresorbable polymers for temporary

therapeutic applications, 1989), (Vert, Li, Spenlehauer, & Guerin, 1992), gave a different definition to the two terms, indicating with the biodegradability the property of a material to be degraded in the biological environment but the degradation products remain in the system, a bioresorbable polymer is completely digested by the immunity system. As stated by Alagusundaram (Alagusundaram.M & S., 2009) the use of bioresorbable polymer has to be preferred since the products of the degradation of the polymer could produce a toxic effect over a long period. For these reason natural polymer are preferred.

The degradation process is of fundamental importance, and is controlled by the characteristics of the polymer.

2.1.4 Microspheres

The microsphere system used for deliver the drug is characterized by a typical diameter in the range of 1 – 1000 μm. The possibility to entrap a large amount of a pharmacological molecule (or protein or growth factor) and the relative easy process for their preparation rend the

polymeric microsphere a very attractive tool for the drug delivery.(Muvaffack, Gurhan, & Hasirci, 2004). Microspheres, furthermore can be direct injected in the targeted site or loaded into the scaffolds for the release of growth factor. (Kawai, Suzuki, Tabata, Ikada, & Nishimura, 2000).

The type of polymer chosen for the microspheres fabrication its molecular weight, the nature of excipients for the stabilization of the drugs and the particle size can potentially compromaise the expected relies profile (Varde & Pack, 2004)

Microsphere size is the discriminating factor for the selection of the method of administration. The microsphere with a diameter less than 6 µm can be injected intravenously (Edlund & Albertsson, 2002). Microsphere with a diameter in the range of 20-100 µm can be administered intramuscular way (Esposito, Cortesi, & Nastruzzi, 1996) or can be subcutaneously injected (Adhirajan, Shanmugasundaram, & Babu, 2007), other interesting application is the intra-articular injection of microsphere with a diameter in the range of 1-70 µm (Larsen, et al., 2008).

2.1.5 Nanoindentation: a mechanical properties assessment

As observed in literature the direct administration of the microspheres has an incisive effect on the restoration of the biological function of the target anatomical district. Furthermore their synergistic combination with other substrate, could enhance the efficiency of scaffolds widely used in tissue or regenerative engineering for the restoration and conservation of tissue functions(Young, 2005). Collocating the microspheres in this field comes out the potentiality of these systems, indeed the development of scaffold with appropriate biocompatibility, biodegradability and, mechanical properties is strictly related to the design of microspheres.

The naoindentaiton technique indeed, is here applied to evaluate the mechanical properties of the microspheres and understand how the polymers adopted for the microsphere fabrication and the cross-linker influence the measured mechanical properties.

2.2 Materials and method

2.2.1 Materials

Two are the polymers used for the microspheres fabrication: Gelatin type A derived through a digestive process of the porcine skin and, chitosan characterized by a molecular weight of 50,000-190,000 Da. The loaded molecule is the methilene blue (MB). All these materials were provided by Sigma-Aldrich. Carlo Erba Reagenti has furnished the acetic acid, the phosphate buffer saline (PBS) has been provided by Gibco Invitrogen Corporation. Wako supplied the Genipin. Upjohn (Kalamazoo Mich, USA) supplied Gelatin Foam (Gelfoam®).

2.2.2 Microspheres fabrication

Water-in-oil emulsion was the method selected for the microsphere preparation. The water was heated at 80 °C and the gelatin powder was added and kindly stirred to achieve the

complete dissolution of the powder. The cross-linking of the gelatin was obtained by using three different concentration of genipin (0.1%, 0.5% or 1% w/v). The new solution was stired at 750 rpm for 1 minute at 80 °C. The solution was then mixed for 30 seconds at 2500 rpm through a vortex mixer.

A 22 G needle fitted in a syringe was used for inject the prepared solution in 200 ml of olive oil preheated at 80 °C. The emulsion was stirred for 1 hour at 800 rpm and maintained at the same temperature.

Chitosan was dissolved in aqueous acetic solultion (1% v/v). The obtained 2% w/v polymeric solution was peocessed with the same proltocol adopted for the production of gelatin microspheres.

Blend of two polymer was used to prepare gelatin-chitosan microspheres. Two different fraction volumes of the prepared solution were mixed in way to obtain 5/1 and 5/3 blend microspheres.

2.2.3 Morphological analysis

The technique of scanning electron microscopy was adopted for the morphological microspheres characterization. Samples were fixed onto metal substrate by using a double sided carbon type and spryed with gold. Through the SEM micrographs the average microspheres diameter was calculated on 100 microspheres randomly selected. For evaluate if prolonged incubation period could introduce modification of microsphere structure, SEM analysis was performed on microspheres previously soaked into PBS and incubated for 10 and 30 days. Before the SEM analysis the microspheres were washed with distilled water and dried.

2.2.4 Micro-compression testing assessment for the mechanical characterization of the microspheres

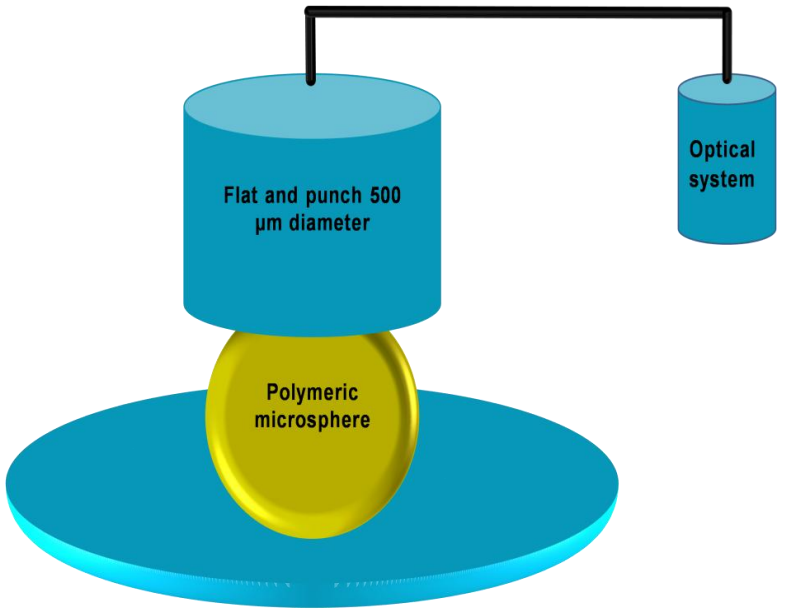

Figure 34: Schematization of the micro-compression test

Micro-compression tests (Figure 34) was performed with the Nanoindenter XP (Agilent/MTS Company), to estimate the mechanical properties of three types of microspheres: gelatin, chitosan and blend 5/1 microspheres.

The theoretical force resolution of the Nanoindenter XP is 50 nN and, the theoretical displacement resolution declared by the producer is lower than 0.01 nm. An ad-hoc protocol for the micro-compression test was developed in way to characterize the mechanical response of the microspheres. The nanoindenter was equipped with a flat end punch of the diameter of 500 μm. Nanoindentation tests starts when the contact between the specimen and the tip is detected. The nanoindentation tests here applied are characterized by three steps: loading, unloading and an hold phase.

During the loading and unloading phases the velocity of the indenter punch was set at a value of 10 nms^{-1}. The hold phase is set in way to stabilize the time dependent phenomenon during which the maximum load was held for a period of 5 s.

The indeintation depth limit was calculated as the 5 % of the initial diameter of the microspheres under investigation measured through the microscope embedded in the nanoindenter.

The load-displacement curve as obtained from the compression tests was analyzed with the Hertz model (2.1)

and the Young's modulus was calculated (Hertz & H, 1882), (Wang, Cowen, Zhang, & Thomas, 2005):

$$P = \frac{4\sqrt{R}}{3}\frac{E}{1-\upsilon^2}\sqrt{\left(\frac{h}{2}\right)^3} \qquad (2.1)$$

Where h is the displacement measured during the compression test R is the radius of the microsphere, P is the load, E is the Young's modulus and υ the Poisson's coefficient. The radius of each tested microsphere was measured trough the optical system of the Nannoindenter XP.

To apply the model to the obtained curves the following hypothesis have been made according to similar works in literature (Lu, Tung, Hung, Shiau, & K-J., 2001):

- The bodies in contact are homogeneous isotropic and linear viscoelastic;
- Volume of the microspheres remains unchanged during the micro-compression test;
- The load is applied only in the normal direction;
- The section of the contact area is circumferential;
- Lateral extension can be considered uniform along the direction of load application and around it;

The Hertz model developed for small deformation and frictionless contact, can be applied to viscous materials only if the load applied can be considered monotonically increasing (Lu, Tung, Hung, Shiau, & K-J., 2001).

Linear regression of the data on the model is performed in way to extrapolate the values of Young's modulus.

First of all the model was linearized in way to apply the procedure of the minimization of the square error. The Hertz model follows a power low so the relation between the load and the displacement can be generalized:

$$P = ah^b \tag{2.2}$$

The constant b assumes, in this case, the value of 1.5 and a can be defined as follow:

$$a = \frac{4R^{\frac{1}{2}}}{3}\frac{E}{1-\upsilon^2}\left(\frac{1}{2}\right)^{\frac{3}{2}} \tag{2.3}$$

Using the logarithm property the relation (2.2) can be linearized:

$$\ln(P) = \ln(a) + \frac{3}{2}\ln(h) \tag{2.4}$$

The linear relation can be written (the subscript i indicates that the data are registered in vectors):

$$l_i = c + \frac{3}{2} d_i \tag{2.5}$$

where:

$$l = \ln(P); \qquad c = \ln(a); \qquad d = \ln(h); \tag{2.6}$$

The error explained by the relation (2.7) (where P is the discrete values registered during the compression test) is minimized respect the constant c:

$$e_i = \left(c + \frac{3}{2} d_i - P_i \right)^2 \tag{2.7}$$

The constant c assumes the following expression:

$$\frac{\partial e_i}{\partial c} = 2 \sum_i \left(c + d s_i - l_i \right) = 0 \quad \Rightarrow \quad c = \frac{1}{n} \sum_{i=1}^{n} l_i - \frac{3}{2n} \sum_{i=1}^{n} s_i \tag{2.8}$$

For the (2.6) the Young's modulus assume the following expression:

$$E = \exp(c)\left[\frac{3R^{-\frac{1}{2}}}{4}\left(\frac{1}{2}\right)^{-\frac{3}{2}}\right] \tag{2.9}$$

For each group of microspheres, 40 indentation tests were carried out. Outliers have been excluded by applying the modified Thompson's Tau method. Young's modulus values obtained have been analyzed with the two way analysis of variance (ANOVA)

2.2.5 Methylene blue loading and characterization of drug release properties of microspheres

PBS solution was adopted for the dissolution of the MB powder (0.1% w/v). The microspheres were soaked with the prepared solution, the suspensions were incubated at 37 °C for one day. The microsphere was dried before the analysis for assess the quantities of MB loaded.

The drug loading potential was evaluated by measuring the MB concentration. The dispersion of the MB molecule was promoted by soaking the microsphere into 10 mL of PBS and ultrasonicated for 1 hour. All the MB loaded was released

repeating the procedure. The ratio between the quantity of MB released and the dry weight of the microspheres, is used for estimate the drug loading.

To obtain the profile release of the drug the microspheres were soaked in 5 mL of PBS and incubated at 37 °C. Periodically samples of the solution were taken for measure the quantities of MB dispersed, the amount of PBS was than replaced to maintain sink conditions. The MB concentration was measured in both the experiments through the UV-Vis Spectrophotometer. The MB release was monitored until all the quantities was released.

2.3 Results and discussions

2.3.1 Morphological analysis

The SEM analysis have revealed that the polymeric microspheres are homogeneous and free of defects Figure 35.

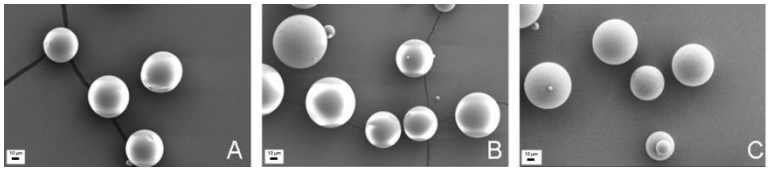

Figure 35: SEM images of gelatin (A), chitosan (B) and blend 5/1 (C). Scale bar 100μm

The average dimensions are listed in the table below:

Table 5: Average diameter of the polymeric microspheres

		Gelatin microspheres Diameter (µm)	Chitosan microspheres Diameter (µm)	Blend 5/1microspheres Diameter (µm)
Genipin concentrartion [% w/v]	0.1	42.7 ± 17.1	54.0 ± 15.9	50.4 ± 19.9
	0.5	44.9 ± 22.1	50.2 ± 22.6	52.3 ± 26.5
	1	53.6 ±24.8	47.1 ± 27.9	52.8 ± 24.9

Statistical analysis do not highlighted significant difference between the groups. The dispersion of the dimension of the microspheres indicates that the used method for their preparation does not allow to obtain a stable formation of microspheres. One of the parameters that influence the

morphology, and so an homogeneous collection of microspheres is the mixing process (Ribatti, Nico, Vacca, & Presta, 2006); as well known the release profile of the drugs is size dependent. The microsphere here obtained, as described in the introduction, can be intramuscular administrated, subcutaneously injected or used for intra-articular drug administration. Also the tissue engineering can benefit of this microspheres since they can be loaded in scaffold in way to gradually release drugs or growth factor (Adhirajan, Shanmugasundaram, & Babu, 2007), (Kojima, Ignotz, Kushibiki, Tinsley, Tabata, & C.A., 2004).

The effect of soaking the microspheres in PBS solution for 10 and 30 days is evaluated trough SEM images. Chitosan and blend microspheres were not affected by any degradation process (images not available). Figure 36 shows, instead, that gelatin microspheres underwent to morphological modification.

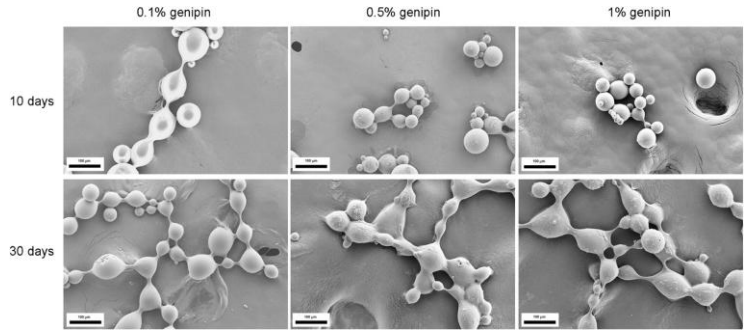

Figure 36*:* SEM analysis of gelatin microspheres soaked in PBS for 10 and 30 days. Scale bar 100μm

The presence of chitosan effectively contribute to stabilize the microsphere structure inasmuch increases the cross-linking degree compared with the gelatin microspheres. In the light of that, the release profile of a DDS can be properly set if the properly polymer is chosen.

2.3.2 Micro-compression tests

Figure 37 shows representative load-displacement curves of the performed nanoindentation tests on single microsphere. An hysteresis loop characterize all the measured curves irrespectively by the percentage of genepin concentration and polymer used for the production of the microspheres, proving

the viscolestic nature of the microspheres. Such type of curves indicates that part of the energy accumulated by the microspheres during the loading phase is dissipated.

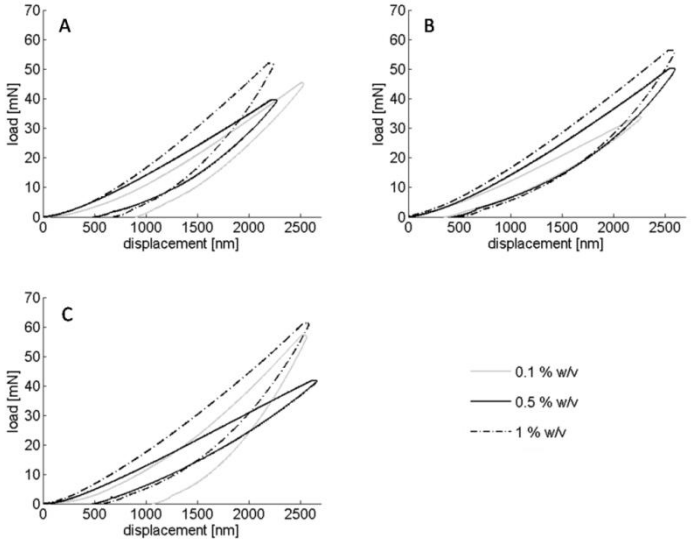

Figure 37: Explicative Load-displacement curves obtained from micro-compression tests performed on gelatin (A), chitosan (B) and blend 5/1(C) microspheres. The data are related to three concentration of genipin cross-linker.

Motion of the polymer chains is the cause of the energy dissipation, it can be concluded that the presence of the hysteresis loop is strictly correlated to the motion of the polymer chains that changes with the degree of cross-linking of the microspheres. This behavior is observed for all the tested microspheres. Similar results (Lieleg, Claessens, Luan,

& Busch, 2008) confirm the found correlation between the energy loss, that is proportional to the amplitude of the hysteresis loop, and the degree of cross-linking i.e. higher is the number of the bonds between the polymer chains and higher is the amplitude of the hysteresis loop.

In the light of what has been observed, and the values reported in the, the area of the hysteresis loop obtained for increasing concentration of cross-linker becomes even more bigger, indicating a stiffening of the microspheres when the cross-linker concentration arise.

Table 6 Energy dissipation values calculated for the three types of microspheres at different cross-linker concentration

Genipin concentration %w/v	Gelatin (mJ)	Chitosam (mJ)	Blend 5/1 (mJ)
0.1	14.07(±6.87)	10.44(±6.79)	14.86(±8.36)
0.5	16.65(±11.28)	20.57(±13.14)	14.48(±9.18)
1	29.12(±14.33)	56.36(±26.43)	28.01(±1.03)

According with the model described in the previous section, the curves were analyzed and a more quantitative characterization of the mechanical properties of the

microspheres was carried out. In Figure 38 the Young's modulus mean values extrapolated by the fitting procedure are shown.

The mean value of the Young's modulus slightly vary between 1.7 GPa (blend 5/1, 0.5 % w/v) and 3.43 GPa (gelatin, 1 % w/v). The statistical analysis highlights that the concentration of the cross-linker and the used polymer for the microspheres fabrication have an impact on their mechanical behavior, even if moderate. For gelatin microsphere further increase of genipin concentration over the 0.5% generate a significantly stiffening of the microspheres. Mechanical properties of chitosan microspheres results in a significantly increasing for cross-linker concentration higher than 0.1%, in this case the role of the cross-linker on defining the stiffness of the microsphere is more marked with respect the gelatin microspheres. The blend 5/1 microspheres are characterized by a counterintuitive related cross-linker trend of the stiffness, the statistical analysis has showed anyway that the genipin concentration affects the mechanical properties of the DDS thus the blending strategy can be used to produce microspheres characterized by mechanical properties tailored for a specific application.

As noticed in previous studies (e.g.,(Long Bi, 2011),(Li Cui, 2014),(GrzegorzGorczyca, 2014)) mechanical properties of cross-linked polymers could depend upon the balance between (1) the degree of cross-linking and (2) the side effect of the cross-linker on the organization of the polymers chain.

Indeed, in the cases of gelatin and gelatin/chitosan blend 5/1 microspheres, the reduction of the Young's modulus as observed by increasing the concentration of genipin from 0.1% to 0.5%, could be ascribed to the modification in the structural disposition of the polymer chains. This structural rearrangement of the polymer chains could be predominant in dictating the mechanical behavior, with respect to the increased number of sites available for cross-linking (which should stiffen the microsphere). With a further increase of genipin concentration beyond 0.5%, cross-linking plays the major role in dictating the mechanical response of the microsphere (as a consequence of the increased degree of cross-linking).

Notably, the not significant difference here observed in the Young's modulus of 0.1 and 0.5% cross-linked gelatin microspheres, lead us to conclude that the side effect of the

cross-linker on the organization of gelatin chains is moderate, even if not negligible.

As for gelatin/chitosan blend 5/1 microspheres, it can be argued that the presence of chitosan emphasizes the counterintuitive trend of the Young's modulus as observed by increasing genepin concentration (a significant difference is observed in the Young's modulus of 0.1% to 0.5% blend microspheres). This observed behavior could be the consequence of the presence of a number of amino groups in chitosan higher than gelatin.

The goodness of the fitting procedure was evaluated by calculating the error between the Hertz model and the experimental data, the mean percentage errors are below the 6.9% indicate that the application of the defined procedure can be successfully applied for the mechanical characterization of these type of microspheres.

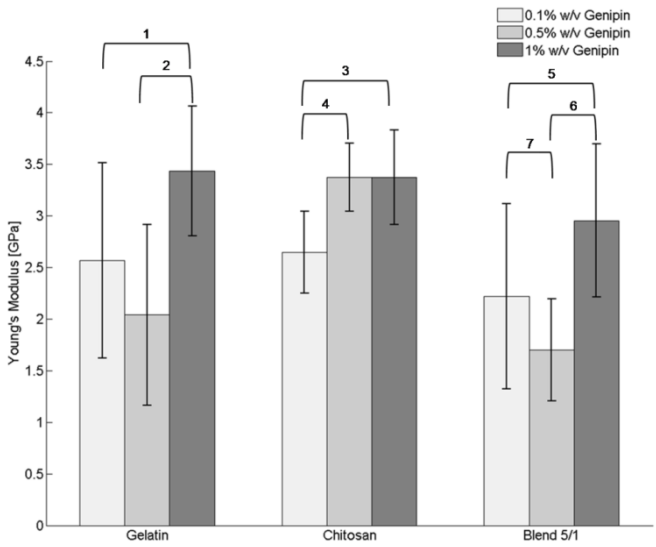

Figure 38*:* Average values of the Young's modulus as obtained for gelatin, chitosan and blend 5/1 microspheres at three different concentrations of genipin. Statistical significant differences ($p<0.05$) between single microsphere preparations with different genipin concentration are also reported. The bars indicate the statistical influence of the cross-linker and the p-values (1-0.0002; 2-$4.87\cdot10^{-7}$; 3-$1.38\cdot10^{-7;}$ 4-$2.32\cdot10^{-9}$; 5-0.0004; 6-$6.23\cdot10^{-11}$; 7-0.0074) obtained for the ANOVA analysis considering a confidence interval of the 95 %.

The proposed mechanical characterization, based on nanoindentation, is applied to the final product, i.e., the microspheres, and not to the rough material used for preparing microspheres. With this approach the the elastic properties of the microsphere was estimated and not the elasticity of the materials used for their fabrication. Nano-indentation has

been applied to generate a stress field able to deform the microsphere in way to evaluate the effect of its internal structure and its shape on the characteristic mechanical properties. Loads required for this analysis are of the order of the magnitude of mN, values that are very far from the loads that an AFM can apply. The implications for this novel strategy are evident, we implemented a test bench able to characterize the final product and not the material before microspheres fabrication. In this regard. The most part of the studies available in the literature do not care about the mechanical behavior of the material used for the microparticles production or, e.g., performing macroscopic characterization of scaffolds functionalized with microspheres (Farnaz Ghorbania, 2016), (Rahmatullah Cholas, 2016). Indeed, attempts to characterize the mechanical behavior of polymeric microspheres have been carried out, in recent years, by applying AFM (Emmanouil Glynos, 2009), (Susheng Tan, 2004). However, it should be reminded here that in the presence of a multiphase material, if a precise value of the hardness of each phase of the material is needed, nanoindenation is the technique to use, AFM being more destined to get a mapping of the surface. In conclusion, AFM is useful for characterization of mechanical properties of the

materials likes polymeric gel and imaging purposes. Moreover, most AFM-based methods focus on estimating elastic properties and neglect viscoelastic behavior, that we demonstrated to be the mechanical behavior of the presented microspheres.

2.3.3 Drug loading and drug release

Analysis conducted on the gelatin and chitosan microspheres for the estimation of the amount of the drug loaded in the microspheres, showed that with the method adopted in this work it is possible incorporate more drug in the gelatin microspheres with respect the chitosan microspheres. The blend microspheres were characterized by an intermediate drug loading potential. Adopting this method the electrostatic interaction between the polymer and the drugs play a significant role, also for the release of the incorporated molecules.

Figure show the cumulative release of the loaded molecules for gelatin, chitosan and blend 5/1 microspheres obtained with 1% of genipin. All the encapsulated molecules were allowed

to be released in way to understand also the therapeutic window associated to the loaded drug.

Modulation of the kinetic release of the drugs is possible by properly regulating the gelatin and chitosan ratio in blend microspheres and, by choosing the polymer taking into account the electrostatic interaction between the drug and polymer. The proof that the electrostatic interaction influence the release kinetic is the prolonged diffusion of the MB molecules for the chitosan microspheres characterized by a positive charge as like as the loaded drugs. The drugs, due to the gradient concentration, should diffuse in the PBS solution but the electrostatic repulsion between the polymer chains and the drug molecules tend to confine the molecules in the microspheres.

The PBS pH of 7.4 makes the gelatin microspheres no electrically charged so it can be supposed that the main mechanism that govern the release of the molecules is the diffusion. As no electrical force oppose to the diffusion of the molecules the release of the MB is very fast.

Blend 5/1 microspheres, as expected, have an intermediate behavior. The observed results indicate that the drug release

kinetic can be controlled by varying the ratio of chitosan/ gelatin.

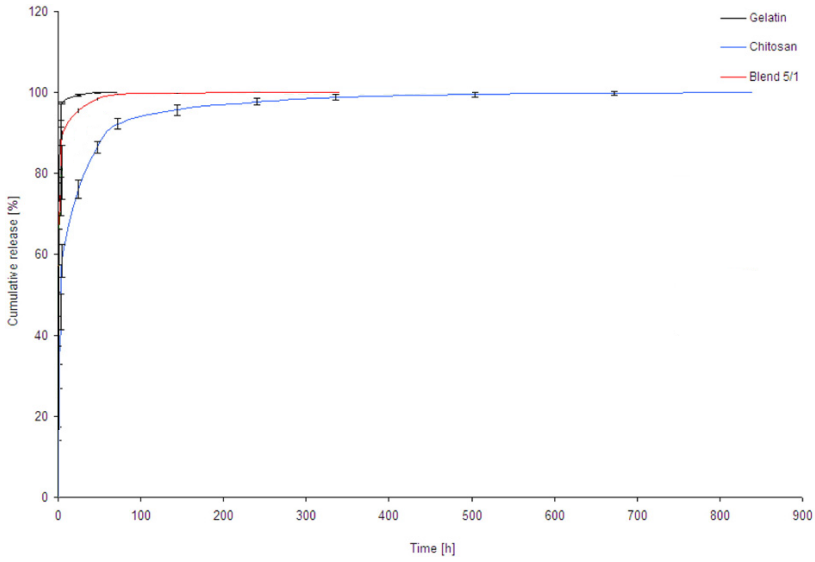

Figure 39: MB release from microspheres cross-linked at 1% genipin concentration

2.4 Conclusion

If the method here used for the microspheres fabrication is well established and largely adopted in literature, the results of the mechanical characterization allow to asses a new

concept that relates the mechanical properties of these kind of DDS and its capacity to release the drugs.

The composition of the polymeric microspheres, does influence their mechanical properties. Drug release experiments, performed by using methylene blue clearly indicate that the time course of the release of the therapeutic agent strongly depends on the used polymer(s). No correlation was found between the mechanical properties of the microspheres and the drug release, indicating that the release kinetic is governed only by chemical mechanisms.

Otherwise more experiments have to be performed, e.g., varying the concentration of genipin, in way to better understand how the degree of cross-linking influence the mechanical properties and consequently the release of drugs.

Finally it can be stated that blending natural polymers and adding genipin as natural cross-linker could lead the production of natural microspheres with adjustable mechanical properties, suitable for drug transport and delivery.

References

Adhirajan, N., Shanmugasundaram, N., & Babu, M. (2007). Gelatin microspheres crosslinked with EDC as a drug delivery system for doxycyline:development and characterization. *J Microencapsul* , 647-659.

Alagusundaram.M, M. S., & S., R. (2009). Microspheres as a novel drug delivery system-A review. *Int.J. ChemTech Res* , 526-534.

Alireza, S., Yasushi, S., Hongbing, L., & Junji, T. (2009). The viscoelastic behaviour of dental adhesives: A nanoindentation study. *Dental Materials* , 13-19.

Allen, M., & Cullis, P. R. (2008). Drug delivery systems: entering the mainstream. *Science* .

Balooch, G., Marshall, G., Marshall, S. W., S.A.S., A., & Balooch, M. (2004). Evaluation of a new modulus mapping technique to investigate microstructural features of human teeth. *J. of biomechanics* , 1223-1232.

Balshakov, A., Oliver, W., & Pharr, G. (1995). Influences of stress on the measuremnt of mechanical properties using nanoindentation: Part II. Finite element simulations. *Journal of materials research* , 760-768.

Bolshakov, A., & Pharr, G. (1998). *J. Mater. Res. 13, 1049* .

Boussineq, J. (1885). Application des Potentiels a l'étude de équilibre et du mouvment des solides élastiques. *Gauthier-Villars* .

Braga, R., Cesa, P., & Gonzaga, C. (2002). Mechanical properties of resin cements with different activation modes. *Journal of Oral Rehabilitation* .

Briscoe, B., Fiori, L., & Pelillo, E. (1998). Nano-indentation of polymeric surface. *J. Phys. D.: Appl. Phys.* , 2395-2405.

Bunton, D. (2002). Generic moves in PhD thesis introductions. In J. Flowerdew, *Academic discourse* (p. 57-75). London: Pearson Education Limited.

Ceballos, L., Miguel, A., Victoria, F., & Jesus, R. (2007). Mechanical characterization of resin cements used for luting fiber posts by nanoindentation. (23).

Chang, L., & Zhang, L. (2009). Mechanical behaviour characterization of silicon and effect of loading rate on pop-in: A nanoindentation study under ultre-low loads. *Material science and Engineering A* , 125-129.

Cheng, Y., & Cheng, C. (2005). *Mat. Sci. Eng. A (409)* .

Cheng, Y., Cheng, C., & Ni, W. (2005). *Mat. Sci. Eng. A (423)* .

Cheng, Y.-T., & Cheng, C.-M. (1998). *J. Appl. Phys. 84, 1284* .

Cheng, Y.-T., & Cheng, C.-M. (1999). *Int. J. Solids Structures 36, 1231* .

Chien-Chao, H., Mao-Kuo, W., & Sanboh, L. (2011). Trensient and steady-state nanoindeintation creep of polymeric materials. *International J. of Plasticity* , 1093-1102.

Chien-Kuo, L., Sanboh, L., Li-Piin, S., & N, T. (2006). Load-displacement relations for nanoindentation of viscoelastic materials. *J. of Applied Physics* .

Cohen, B., Pagnillo, M., Newman, I., Musikant, B., & A.S., D. (1998). Retention of three endodontic posts cemented with five dental cements. *J Prosthet Dent.* , 520-525.

Dias, A. A., & Hendriks, M. (2001). Perfect polymers, Controlled release.

Doerner, M., & Nix, W. (1986). A method for interpreting the data from depth-sensing indentation instruments. *J. Mater. Res.* , 601-609.

Edlund, U., & Albertsson, A. (2002). Degradable polymer microspheres for controlled drug delivery. *Advances in polymer science [1965]: Degradable aliphatic polyesters* , 67-112.

Egle Saskalauskaite, L. E. (2007). Flexural Strength, Elastic Modulus, and pH Profile of Self-etch Resin Luting Cements. *Journal of prosthodontics* .

Emmanouil Glynos, V. K. (2009). Nanomechanics of Biocompatible Hollow Thin-Shell Polymer Microspheres, . *Langmuir* , 7514-7522.

Esposito, E., Cortesi, R., & Nastruzzi, C. (1996). Gelatin microspheres: influence of preparation parameters and thermal treatment on chemico-physical and biopharmaceutical properties. *Biomaterials* , 2009-2020.

Farnaz Ghorbania, H. N. (2016). Physicochemical and mechanical properties of freeze cast hydroxyapatite-gelatin scaffolds with dexamethasone loaded PLGA microspheres for hard tissue engineering applications. *Materials Science and EnginMaterials Science and Engineering: C* , 208–220.

Feng, G., & Ngan, A. (2001). Creep and strain burst in indium and aluminum during indentation . *Scripta Materialia* , 971-976.

GrzegorzGorczyca, R. T. (2014). Preparation and characterization of genipin cross-linked porouschitosan–

collagen–gelatin scaffolds using chitosan–CO2solution. *Carbohydrate Polymers* , 901-911.

Hamdi, G., Ponchel, G., & Duchene, D. (1998). An original method for studying in vitro the enzymatic degradation of crosslinked starch microspheres. *Journal of Controlled Release* , 193-201.

Harsha, S., & Rani, R. H. (2006). Drug targeting to lungs by way of microspheres. *Arch. Pharm. Res.* , 598-604.

Harsha, S., Chandramouli, R., & Rani, S. (2009). Ofloxacin targeting to lungs by way of microspheres. *International Journal of pharmaceutics* , 127-132.

Hay, J., Bolshakov, A., & Pharr, G. (1999). *J. Mater. Res. 14, 2296* .

Hertz, & H. (1882). Uber die Beruhrung tester Elastische Korper und Uber die Harte (On th Contact of Rigid Elastic Solids and on hardness) Verhandlungen des Vereinszur Beforderung des (For English translation see Miscellaneous Papers by H Hertz, Eds. Jones an.

Hertz, H. (1882). Reine und angewandte Mathematik.

Hochstetter, G., Jimenez, A., & Loubet, J. (1999). Strain-Rate Effects on hardness of Glassy Polymers in the Nanoscale Range. Composition Between Quasi-Static and Continuous Stiffness Measurement. *J. Macromol. Sci.- Phys.* , 681-692.

Hofmann, N., Papsthart, G., Hugo, B., & Klaiber, B. (2001). Comparison of photo-activation versus chemical or dual-curing of resin-based luting cements regarding flexural strength, modulus and surface hardness. *J Oral Rehabil.* , 1022-1028.

Horieh, M., Ilnaz, H., Alireza, S., Suppason, T., & Junji, T. (2013). Effects of curing mode and moisture on nanoindentation mechanical properties and bonding of a self-adhesive resin cement to pulp chamber floor. *Dental Materials* , 708-717.

James, L. (2005). Nanoindentation of Dental Composites. *J. of Biomedical Materials Research Part B: Applied Biomaterials* , 27-34.

Kawai, Suzuki, S., Tabata, Y., Ikada, Y., & Nishimura, Y. (2000). Accelerated tissue regeneration through incorporation of basic fibroblast growth factor-impregnated gelatin microspheres into artificial dermis. *Biomaterials* , 489-499.

Kim, Y., Yamashita, J., Shotwell, J., Chong, K., & Wang, H. (2006, June). The comparison of provisional luting agents and abutment surface roughness on the retention of provisional implant-supported crowns. *the Journal of Prosthetic Dentistry , 95* (6).

King, R. (1987). *Int. J. Solids Struct. 23, 1657* .

Kojima, K., Ignotz, R., Kushibiki, T., Tinsley, K., Tabata, Y., & C.A., V. (2004). Tissue-engineered trachea from sheep

marrow stromal cells with transforming growth factor β2 released from biodegradable microspheres in a nude rat recipient. *J. Thorac. Cardiova* , 147-153.

Kwan, B. S. (2009). Reading in preparation for writing a PhD thesis: Case studies of experiences. *Journal of English for Academic Purposes* , pages 180-191.

Larsen, C., Ostergaard, J., Larsen, S., Jensen, H., Jacobsen, S., Lindegaard, C., et al. (2008). Intra-articular depot formulation principles:role in the management of postoperative pain and arthritic disorders. J Pharm Sci, 97, 4622–4654. *J. Pharm. Sci.* , 4622-4654.

Larsson, P.-L., Giannakopoulos, A., Soderlund, E., Rowcliffe, D., & Vestergaard, R. (1996). *Int. J. Solids Structures 33, 221* .

Li Cui, J. Y. (2014). Preparation and characterization of IPN hydrogels composed ofchitosan and gelatin cross-linked by genipin. *Carbohydrate Polymers* , 31-38.

Lieleg, O., Claessens, M., Luan, Y., & Busch, A. (2008). Transient binding and dissipation in cross-linked actin networks. *Phys. Rev. Lett.* .

Li-Hong, H., & Michael, V. (2008). Nanoindentation creep behavior of human enamel. *J. of Biomedical Materials Research Part A* .

Liu, C.-K., & Lee, S. (2006). Load-displacement relations for nanoindentation of viscoelastic materials. *Journal of Applied Physics* .

Lixian, Z., Longquan, S., L., L., & Danyu, J. (2016). An abnormal displacement change during holding period in nanoindentation tests on zirconia dental ceramic. *Journal of advanced ceramics* , 153-158.

Long Bi, Z. C. (2011). Effects of different cross-linking conditions on the propertiesof genipin-cross-linked chitosan/collagen scaffolds for cartilagetissue engineering. *J Mater S Mater Med* , 51-62.

Love, A. (1939). Boussinesq's problem for a rigid cone.

Lu, W., Tung, K.-L., Hung, S.-M., Shiau, J.-S., & K-J., H. (2001). Compression of deformable gel particles. *Powder Technology* , 1-12.

Lucas, B., Oliver, W., Pharr, G., & Louber, J.-L. (1997). Time Dependent Deformation During Indentation Testing. *Mat. Res. Soc. Symp. Proc. 436* , 233-238.

Mahalia, M., Christopher, B., Matthieu, V., & Franz-Josef, U. (2008). Surface roughness criteria for cement paste nanoindentation. *Cement and Concrete Research* , 467-476.

Marezan, P., Beyaoui, M., Bigerelle, M., & Guigon, M. (2012). Dtermination of mechanical properties by nanoindentation in the case of viscous materials. *Int. J. Mat. Res.* , 715-722.

Martinho, N., Damgé, C., & Reis, C. P. (2011). Recent advances in drug delivery systems. *Journal of biomaterials and nanobiotechnology* , 510-526.

Muvaffack, A., Gurhan, I., & Hasirci, N. (2004). Wiley Periodicals. *Prolonged cytotoxic effect of colchicine released from biodegradable microspheres* .

Ohyoung, K., & Jaewoo Shim, W. (2001). Studies on the Preparation and Mechanical Properties af Esthatic Poolymeric Dental Restoratives Using Silane Treated Silica Microfillern via Frezze-Drying. *Polymer Composites* , 650-659.

Olesiak, S., & Oyen, L. (2010). Viscous-elastic-plastic behavior of bone using Berkovich nanoindentaiìtion. *Mech. Time-Dependent Mater.* , 111-124.

Oliver, W., & Pharr, G. (1992). An improved technique for determining hardness and elastic modulus using load and displacement sensing indentation experiments. *J. Mater. Res.* , 1564-1583.

Oliver, W., & Pharr, G. (1992). An improved technique for determining hardness and elastic modulus using load and displacement sensing indentation experiments. *J. Mater. Res.* , 1564-1583.

Oliver, W., & Pharr, G. (2004). Measurement of hardness and elastic modulus by instrumented indentation: Advances in understanding and refinements to methodology. *Journal of Materials Research* , 3-20.

Oyen, L., & Cook, R. (2003). Load-displacement behavior during sharp indentation of viscous-elastic-plastic materials. *J. Mater. Res* , 139-150.

Oyen-Tiesma, M., Tivola, Y., & Cook, R. (2001). Load-displacement Behaviour During Sharp Indentation of Viscous-Elastic-Plastic Materials. *Mat. Res. Soc. Symp.*

Pan, Y., & Lin, C. (2005). The effect of luting agents on the retention of dental implant-supported crowns. *Chang Gung Med J.* , 403-410.

Peluccio, M., Bignardi, C., Lombardo, S., F.M., M., & Carossa, S. (2007). Comparative study of nanomechanical properties of cements used in teeth restoration. *J. of Physics Condensed Matter* , 1-10.

Petrak, K. (2005). Essential properties of drug-targeting delivery systems, Reviews. *Drug discovery today* .

Rahmatullah Cholas, S. K. (2016). Scaffolds for bone regeneration made of hydroxyapatite microspheres in a collagen matrix. *Materials Science and Engineering: C* , 499-505.

Ranade, V.V., & Cannon, J. (third edition, 2011). *Drug delivery systems.*

Ribatti, D., Nico, B., Vacca, A., & Presta, M. (2006). The gelatin sponge-chorioallantoic membrane assay. *Nat. Protoc.* , 85-91.

Ronald L., S., & John M., P. (2012). *Craig's restorative dental materials.* Philadelpia: Elsevier.

Samad, A., Sultana, Y., & Aqil, M. (2007). Liposomal drug delivery systems: an update review. *Current drug delivery* , 297-305.

Sanjay, V. (2001). Current status of drug delivery technologies and future directions. *Pharmaceutical technology on-line* , 4.

Schuh, C. (2006). Nanoindentation studies of materials. *Materials today* , 32-40.

Schwendener. (2007). *Liposomes in biology and medicine.*

Sheets, J., Wilcox, C., & Wilwerding, T. (2008). Cement selection for cement-retained crown technique with dental implants. *J Prosthodont.* , 92-96.

Sneddon, I. I. (1965). The ralation between load and penetration in the axisymmetric Boussinesq problem for a punch of arbitrary profile. *Int. J. Engng Sci.* , 47-57.

Susannah K., T., Oana R., G., M.Hooper, & Kenneth E., E. (2007). Monomer conversion and hardness of novel dental cements based on ethyl cyanoacrylate. *Dental Materials* , 799-806.

Susheng Tan, R. L. (2004). Nanoscale Compression of Polymer Microspheres by Atomic Force Microscopy. *Langmuir* , 7015-7020.

Tabor, D. (1948). *Proc. R. Soc. A 192, 247* .

Tang, B., & Ngan, A. (2003). *J. Mater. Res. 18* , 1141.

Tiwari, G., Tiwari, R., B., S., Pandey, L., & Saurabh, P. (2012 , 2 (1)). Drug delivery systems: an updated review. *Int J Pharm Investig.* , 2-11.

Toparli, M., & N.S., K. (2005). hardness and yield strength of dentin from simulated nano-indentation tests. *Computer Methods and Programs in Biomedicine* , 253-257.

Tsui, T., Oliver, W., & Pharr, G. (1995). Influences of stress on the measurement of mechanical properties using nanoindentation: Part1. Experimental studies in an aluminum alloy. *Journal of Material researc* , 752-759.

Varde, N. K., & Pack, D. (2004). Microspheres for controlled release drug delivery. *Opin. Biol. Ther.* , 35-51.

Vert, M. (1989). Bioresorbable polymers for temporary therapeutic applications. *Die Angewandte makromolekulare Chemie* , 155-168.

Vert, M., Li, S. M., Spenlehauer, G., & Guerin, P. (1992). Bioresorbability and biocompatibility of aliphatic polyesters. *Journal of materials science. Materials in medicine* , 432-446.

Vilar, T.-P. J., & Albericio, F. (2012). Polymers and Drug Delivery Systems. *Current Drug Delivery* .

Vladislav, D., Gogotsi, Y., & Dub, S. (2000). Effect of phase tranformation on the shape of the unloading curve in the nanoindentation of silicon. *Appl. Phys. Lett.* , 2214-2216.

Wang, C., Cowen, C., Zhang, Z., & Thomas, C. (2005). High speed compression of single alginate microspheres. *Chem. Eng. Sci.* , 6649–6657.

Whittaker, M., Harrison, W., Deen, C., Rae, C., & Williams, S. (2017). Creep Deformation by Dislocation Movement in Waspaloy. *Materials* , 1-14.

Yoldas, O., & Alaçam, T. (2005). Microhardness of composites in simulated root canals cured with light transmitting posts and glass-fiber reinforced composite posts. *J Endod* , 104-106.

Young, S. W. (2005). Gelatin as delivery vehicle for the controlled release of bioactive molecules. *Journal of controlled release* , 256-274.

Zhang, L., Shao, L., Li, L., & Jiang, D. (2016). An abnormal displacement change during holding period in nanoindentation tests on zirconia dental ceramic. *Journal of Advanced Ceramics* , 153-158.

Zhang, Y., Chan, H., & Leong, K. (2013). Advanced materials and processing for drug delivery: The past and the future, Advanced drug delivery reviews. 104-120.

Zhang, Y., Ouyang, H., Lim, C., Ramakrishna, S., & Huang, Z. (2005). Electrospinning of gelatin fibers and gelatin/PCL composite fibrous scaffolds. *J Biomed Mater Res B Appl Biomater* , 156-165.

Zhi-Quiang, F., Qi-Chang, H., Quingfeng, Z., & Pierre, J. (2010). Theory of Nanoindentation. *Handbook of Nanophysics* , 1-15.